

Structural Analysis and Optimization of a UAV wing

João Francisco Matos Alves Ferreira

Thesis to obtain the Master of Science Degree in

Mechanical Engineering

Supervisors: Prof. Virgínia Isabel Monteiro Nabais Infante

Prof. José Firmino Aguilar Madeira

Examination Committee

Chairperson: Prof. Luís Filipe Galvão dos Reis

Supervisor: Prof. José Firmino Aguilar Madeira

Member of the Committee: Prof. Rui Miguel Barreiro Ruben

November 2018

To my family for all the unconditional support over these 23 years.

Acknowledgments

I would like to say thanks to all the people that contributed for this work and to all the ones that help me during my academic path:

To the “UAVision” company for allowing me to develop this work.

To my master’s thesis supervisor’s professor Virgínia Infante and professor José Aguilar, for all the support, knowledge, patience and guidance during this work.

To the aerospace engineer Diogo Vicente, from “UAVision”, for all the patience, knowledge and commitment during this work.

To professor Miguel Neves and professor Luís Sousa for the knowledge and tools provided during this work.

To my friends Jorge, Nuno, João, Francisco, Shu and Pedro, for all the friendship and solidarity over these 5 years.

To my friend Francisco Vieira for all the engineering knowledge.

To my grandparents for all the love and support.

To my father Jorge, my mother Helena, my older sister Rita and my younger sister Maria for all the love, advice, investment, knowledge and patience.

Resumo

O uso de veículos não tripulados, conhecidos como UAVs, são extremamente úteis em missões ambientais como por exemplo na medição dos gases emitidos por um navio em alto mar, acidentes marítimos e incêndios florestais. Uma vez que são controlados à distância, apresentando uma boa autonomia, agilidade e segurança, este tipo de veículos vêm acrescentar uma eficácia nos resultados deste tipo de missões. Os materiais compósitos desempenham um papel importante na estrutura destes veículos, sendo a otimização estrutural uma necessidade constante, nomeadamente das asas.

Este trabalho foi desenvolvido juntamente com a empresa “UAVision”, fazendo-se a análise estrutural e otimização topológica da asa de um dos seu UAVs. O objetivo principal deste trabalho é a utilização do método de otimização multiobjetivo “direct multisearch” (DMS), de modo a minimizar a deflexão máxima da asa e a sua massa, com o intuito de melhorar a estabilidade de voo e a autonomia do veículo, respetivamente. O método DMS usa o conceito de “dominância de Pareto” para definir a lista de pontos não dominados, de onde as novas iterações são escolhidas.

Utilizando o software comercial *ANSYS Mechanical APDL 18.1* foi criado um modelo em 3D da asa, com base nas dimensões da atualmente comercializada (modelo *Solidworks*, cortesia de “UAVision”). Foi feita uma análise aerodinâmica assumindo condições de voo estacionário, utilizando o software *XFLR5*, de modo a obter o perfil de forças aplicadas na asa. Para a otimização topológica, foi utilizado o software *MATLAB R2015a* (usando o DMS).

Com este trabalho determinaram-se 17 geometrias de asa aceitáveis, atingindo-se uma diminuição máxima de 0.3 % da deflexão máxima da asa e de 8 % da massa da asa.

Palavras Chave: UAV, asa, análise estrutural, materiais compósitos, DMS, otimização multiobjetivo

Abstract

The use of unmanned aerial vehicles, also known as UAVs, are extremely useful on environmental operations such as on the measure of the gases emitted by a boat, in maritime accidents and in forest fires. By being controlled from a distant point, having a reasonable autonomy and agility, those vehicles came to add an efficiency on the results of those operations. It is also a safer procedure where there are no human lives in danger. The composite materials play a key role in the UAVs structure, being its optimization a real need, namely in the wings.

The present study was developed with “UAVision”, doing the structural analysis and topology optimization of the wing of one of theirs UAVs. The main goal is to implement the optimization multiobjective derivative-free method called “direct multiseach” (DMS), to minimize the maximum deflection and mass of the wing, to improve the autonomy of the vehicle and its flight stability. The DMS solver uses the concept of Pareto dominance to define a list of nondominated points, from which the new iterates are chosen.

A 3D model based on the current wing dimensions (*SolidWorks* model, courtesy of “UAVision”) was built from scratch, using the commercial software *ANSYS Mechanical APDL 18.1*. Assuming stationary flight conditions, was used the *XFLR5* software to obtain the distributed lifting forces to apply on the wing. For the topology optimization was used the *MATLAB R2015a* software (using the DMS).

Was achieved 17 acceptable wing geometries, reaching a maximum decrease of 0.3% of the maximum wing deflection and 8% of the wing mass.

Keywords: UAV, wing, structural analysis, composite materials, DMS, multiobjective optimization

Contents

Acknowledgments	i
Resumo	iii
Abstract.....	v
List of Tables	ix
List of Figures	xi
Nomenclature	xv
1 Introduction	1
1.1 Scope	1
1.2 Objectives.....	3
1.3 Methodology.....	4
1.4 Structure of the thesis.....	5
2 State of Art.....	6
2.1 Composite Materials.....	6
2.1.1 Definition.....	6
2.1.2 Types of composite materials and their components.....	6
2.1.3 Advantages and disadvantages	8
2.1.4 Carbon-epoxy composites.....	9
2.1.5 Applications in the aerospace industry	9
2.2 The use of UAVs nowadays.....	11
2.2.1 Environmental and rescue missions	12
2.2.2 Military applications.....	13
2.2.3 Other applications	13
2.3 Optimization	14
2.3.1 Topology optimization	14
2.3.2 Multiobjective optimization	15
2.3.3 Direct Multisearch (DMS)	17
2.4 Previous optimization works	18
3 Numerical Simulation	22
3.1 ANSYS Mechanical APDL model	22
3.1.1 Introduction	22
3.1.2 Conceptualization of the model	22
3.1.3 Mesh and boundary conditions.....	24
3.1.4 Materials	26

3.1.3 Young's modulus calculation	30
3.1.4 Output	33
4 Optimization	34
4.1 Introduction.....	34
4.2 Design variables	35
4.2.1 X position of the spars.....	35
4.2.2 No. Laminas, fiber orientation and material thickness	36
4.3 MATLAB and ANSYS Mechanical APDL	37
4.3.1 MATLAB functions	37
4.3.2 Functionality.....	38
4.3.3 Results from the optimization point of view.....	39
5 Results.....	40
5.1 Wing test made in "UAVision"	40
5.1.1 Characteristics of the wing	40
5.1.2 Particularities of the test	41
5.2 Numerical simulation and optimization results	42
5.2.1 Characteristics of the wing before the optimization.....	42
5.2.2 Interpretation of the results.....	44
6 Production of the Wing.....	52
6.1 Wing components	52
6.2 Assembly	53
7 Conclusions and Future Works	55
References	57
Annexes.....	61

List of Tables

Table 1 - Advantages vs disadvantages of composite materials [14].....	8
Table 2 - Dimensions of the Specimens [36].....	27
Table 3 - INSTRON 2630-106 specifications [42].....	28
Table 4 - Values of the calculations to obtain the young's modulus.....	31
Table 5 - Young's modulus values.....	31
Table 6 - Carbon - epoxy properties [8].....	32
Table 7 - "Airex C70.75" properties [9].....	32
Table 8 - Aluminum 6082 T6 properties [10].....	32
Table 9 - Optimization design variables x_i	34
Table 10 - <i>MATLAB</i> functions.....	37
Table 11 - Information about the wing geometry currently used (courtesy of "UAVision").....	43
Table 12 - Objective functions values of the current wing geometry (<i>ANSYS</i> simulation).....	44
Table 13 - Wing geometry characteristics of point A, B and C.....	47
Table 14 - Results remarks.....	48

List of Figures

Figure 1 - UAV in study [5].....	2
Figure 2 - External dimensions of the wing (<i>mm</i>) [5].....	3
Figure 3 - Work methodology.....	4
Figure 4 - Qualitative comparison: Composite materials vs monolithic materials [12].....	6
Figure 5 - Load transfer and stress distribution in a composite subjected to an axial load [13].....	6
Figure 6 - Some types of fiber-reinforced laminas [13].....	7
Figure 7 - Boeing 787 structural materials [14].....	10
Figure 8 - Structural weight of carbon-epoxy composite vs metals [19].....	11
Figure 9 - Structural components of a UAV wing (courtesy of “UAVision”).....	11
Figure 10 - Carbon-epoxy arm and rotor blades (courtesy of “UAVision”).....	11
Figure 11 - A firefighting UAV [25].....	13
Figure 12 - a) sizing optimization; b) shape optimization; c) topology optimization [26].....	14
Figure 13 - Feasible criterion space [29].....	15
Figure 14 - Pareto front for 4 different objective functions combinations [30].....	16
Figure 15 - 3D wing model (<i>ANSYS</i> model).....	23
Figure 16 - UAV wing (courtesy of “UAVision”).....	23
Figure 17 - Interior of the 3D wing model (<i>ANSYS</i> model).....	23
Figure 18 - Division of the lines to generate the mesh (<i>ANSYS</i> model).....	24
Figure 19 - Mesh (<i>ANSYS</i> model).....	24
Figure 20 - 3D wing model (<i>XFLR5</i>).....	25
Figure 21 - Loads from <i>XFLR</i> applied on the wing (<i>ANSYS</i> model).....	25
Figure 22 - Symmetry and fixed end boundary conditions (<i>ANSYS</i> model).....	26
Figure 23 - Sheet of 2x2 twill weave carbon fiber (courtesy of “UAVision”).....	27
Figure 24 - Haas VF-4SS used to cut the specimens (courtesy of “UAVision”).....	27
Figure 25 - INSTRON 2630-106 (courtesy of “Técnico Lisboa”).....	28
Figure 26 - INSTRON 5566 (courtesy of “Técnico Lisboa”).....	29
Figure 27 - Experimental data example.....	29

Figure 28 - Carbo-epoxy specimens after the tensile test (courtesy of “Técnico Lisboa”).....	30
Figure 29 - Output ".txt" file.....	33
Figure 30 - Winglet tip where the maximum deflection is measured (ANSYS model).....	33
Figure 31 - Composition of the composite based structural components.....	35
Figure 32 - Wing airfoil (front view) and the coordinated axis (ANSYS model).....	36
Figure 33 - Spars, ribs and winglet (ANSYS model).....	36
Figure 34 - Functionality of the optimization procedure.....	38
Figure 35 - “funcFF.m” function.....	38
Figure 36 - The total nondominated solutions.....	39
Figure 37 - Internal structure of the UAV wing tested (courtesy of “UAVision”).....	40
Figure 38 - Exterior of the UAV wing tested (courtesy of “UAVision”).....	40
Figure 39 - UAV wing test (courtesy of “UAVision”).....	41
Figure 40 - Lift loads distribution in an aircraft wing [44].....	41
Figure 41 - Current UAV wing geometry <i>SolidWorks</i> model (courtesy of “UAVision”).....	42
Figure 42 - Carbon-epoxy tubes (courtesy of “UAVision”).....	42
Figure 43 - Aluminum rib in the real wing (courtesy of “UAVision”).....	43
Figure 44 - Aluminum rib in the ANSYS model.....	44
Figure 45 - All the possible solutions.....	45
Figure 46 - Possible solutions acceptable.....	46
Figure 47 - Position of the spars, point A, B, C (ANSYS model).....	48
Figure 48 - Tensile stress values of spar 5, point A (ANSYS model).....	49
Figure 49 - Tensile stress values of spar 5, point B (ANSYS model).....	50
Figure 50 - Maximum tensile stress value, point A (ANSYS model).....	50
Figure 51 - Maximum tensile stress value, point B (ANSYS model).....	51
Figure 52 - Maximum tensile stress value, point C (ANSYS model).....	51
Figure 53 - Wing molds (courtesy of “UAVision”).....	52
Figure 54 - Robot (courtesy of “UAVision”).....	53
Figure 55 - Mechanical lathe (courtesy of “UAVision”).....	53
Figure 56 - Carbon-epoxy room (courtesy of "UAVision").....	54

Figure 57 - Painting room (courtesy of “UAVision”).....54
Figure 58 - Certification of attendance at EngOpt2018.....61

Nomenclature

Abbreviations

ASTM – American Society for Testing Materials
DMS – Direct Multisearch
DoF – Degrees of Freedom
FEA – Finite Elements Analysis
FEM – Finite Elements Method
GLODS - Global and Local Optimization using Direct Search
MOO – Multi-objective optimization
MOUT – Military Operations in Urban Terrain
SaR – Search and rescue
UAS – Unmanned Aerial System
UAV – Unmanned Aerial Vehicle

Symbols

A – initial cross section area
 E – young's modulus
 $f_k(x)$ – objective function
 F – tensile load
 $g_j(x)$ – inequality constraints
 G – shear modulus
 $h_i(x)$ – equality constraints
 k – number of objective functions
 m – number of inequality constraints
 p – number of equality constraints
 Z – feasible criterion space

ϵ – strain
 σ – tensile stress

ν – poisson's ratio

ρ – density

Ω – feasible region

1 Introduction

1.1 Scope

The Unmanned Aerial Vehicles (UAVs), as it is defined in [1], are “aerial vehicles that do not carry a human operator, use aerodynamic forces to provide vehicle lift, can fly autonomously or be piloted remotely, can be expendable or recoverable, and carry a lethal or nonlethal payload.” They can be powered by several types of engines, such as combustion (the case of this work) and electrical engines. Those type of vehicles are not new in the engineering field. Actually, the first kind of pilotless object was developed in 1918, in a military environment as a type of long-range artillery [2]. As it is commonly seen in the technological evolutionary process, in the case of the UAVs, the wars had a key role: from the WWII to the most recent ones, such as Iraq (2003), Afghanistan (2001) and Kosovo (1999) [1,2].

Besides the military applications, the truth is that UAVs perform an extensive number of civil tasks, namely environmental. Nowadays, problems such as oil splits and forest fires are a real problem, and the prevention and control of those accidents are extremely important. In that conditions, UAVs are a reliable and safe alternative to accomplish the tasks successfully [3,4]. Another interesting application is the control of the gases emitted by a ship when it is in operation. Being it a dangerous task for a person, the importance of the UAVs is highlighted again. This last application is the core goal for the UAV in study, Figure 1.

It is important to refer the cost reduction in production, maintenance and operation of those vehicles as well as its maneuverability, when compared with the traditional manned piloted aircrafts [3].

In this way, to achieve the best results, the design and the optimization of the different components of the UAVs are extremely important, namely the wings. Based on [6], a wing can be compared with a beam that transmits and gathers all the applied air load to the fuselage. Its structural role is primordial for a stable and functional flight. Some considerations such as high lifting force, low aerodynamics drag and low mass, are constraints that should be fulfilled when designing a wing. Respecting that fact, the choice of the materials is another important step to achieve the optimal performance. Materials such as aluminum and carbon-epoxy composites, with strong mechanical properties, contribute to the “strength, stiffness and light weight structure” [6] required for the wings of this type of aerial vehicles.



Figure 1 - UAV in study [5]

The present work was made in collaboration with the “UAVision” company. “UAVision” is a Portuguese company, founded by alumni from “Técnico Lisboa” in 2005. Nowadays they are “experts in development, production and marketing of fixed-wing and multi-rotors” UAVs. They also design and produce some sensors for different applications and other kind of technological innovations like “instrumented buoys for monitoring of the sea and environmental parameters”. Their UAVs have been using in different countries, in military, environmental and civil applications. The big majority of the electronics and structural components of their products are developed and manufactured in their premises (address: Casais da Arriota, 26 Bonabal 2565-835 Ventosa Portugal) [5].

The company has a multidisciplinary team that covers different engineering areas, such as “aerospace, electronics, mechanical, automation and control, and image processing”. They work mainly with carbon composite materials. The team is able to design, simulate and test all the sub-systems of an UAV, from the structural components to the navigation and control algorithms [5].

“UAVision” works closely with universities and research centers like “Técnico Lisboa”. This work is an example of that, an eight-months collaboration with the supervision and help of the aerospace engineer Diogo Vicente, who demonstrated an extensive engineering knowledge and experience. His availability, inside and outside of the company, was fundamental for the success of this work. During this learning time experience, the *ANSYS Mechanical APDL* model was built from scratch. It was possible to follow the company routines and all the design and manufacture process of their products [5]. The kindness of the workers and the good environment of the company made this experience gratifying and useful from the engineering point of view.

Besides all the products, “UAVision” provides a “UAV training service” dedicated to the UAV training needs. They provide it to both internal and external pilots (fixed-wing or multi-rotors UAVs) as well as to payload operators and tactical missions. This training service can be personalized based on the needs [5]. For more information, is advisable to consult [5].

Some details about “UAVision” will be mentioned and assumed along this document.

The component in study is the wing. The structural analysis was based on the dimensions imposed by the company (*SolidWorks* model, courtesy of “UAVision”), as well as the materials, since it is expected to produce the optimal version of the wing with the resources available. Because of that, it was made a topology optimization, being the external geometry of the wing preserved. The overall dimensions are showed in Figure 2. The structure is constituted by several ribs, some spars, two winglets and some internal and external holes for the electrical and other structural components.

It was used three software in this work: *ANSYS Mechanical APDL 18.1* to the 3D modelling and structural analysis of the UAV wing (the geometry of the wing was simplified and based on the *Solidworks* model); *MATLAB R2015a* to the application of the “direct multisearch” (DMS) solver (optimization) and *XFLR5* to obtain the distributed lifting forces.

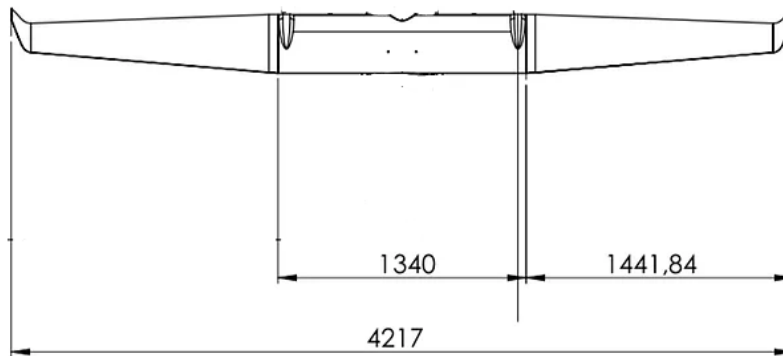


Figure 2 – External dimensions of the wing (mm) [5]

1.2 Objectives

The main goal of this work is to optimize topologically the wing, using the “direct multisearch” solver (DMS) [7], minimizing the maximum deflection of the wing and its mass value.

Since the materials are the available ones in the “UAVision” company (the same already being used), the mass can be reduced manipulating the thickness of the materials and the number of laminas in the carbon-epoxy composite components. Based on that and modifying the positions

of the structural internal reinforcements (spars), the value of the maximum deflection changes. Having the minimization of the deflection and mass balanced, is possible to achieve an optimal structure. It is important to refer that having a lower structural weight allows an increase in the autonomy of the UAV and consequently a reduction in some cost (less material, less fuel consumed, etc). Having a controlled wing deflection value, the flight will be more stable and the structure more reliable.

1.3 Methodology

To accomplish the objectives, a structural linear elastic analysis of the UAV wing and its 3D model (half of the wing) was done using the *ANSYS Mechanical APDL* software. Related to the boundary conditions assumed, the *XFLR5* software was used to find the distributed lifting forces to apply on the wing. Besides that, a fixed end and a symmetry boundary conditions were considered in the half wing tip that connects to the fuselage. The topology optimization was ensured by the “direct multisearch” solver (DMS). A derivative free method that executes a local search around a poll center and uses the concept of Pareto dominance to define a list of nondominated points, from which the new iterates are chosen. The *ANSYS* model was incorporated in the DMS solver.

Figure 3 shows, in a schematic way, the methodology of this work.

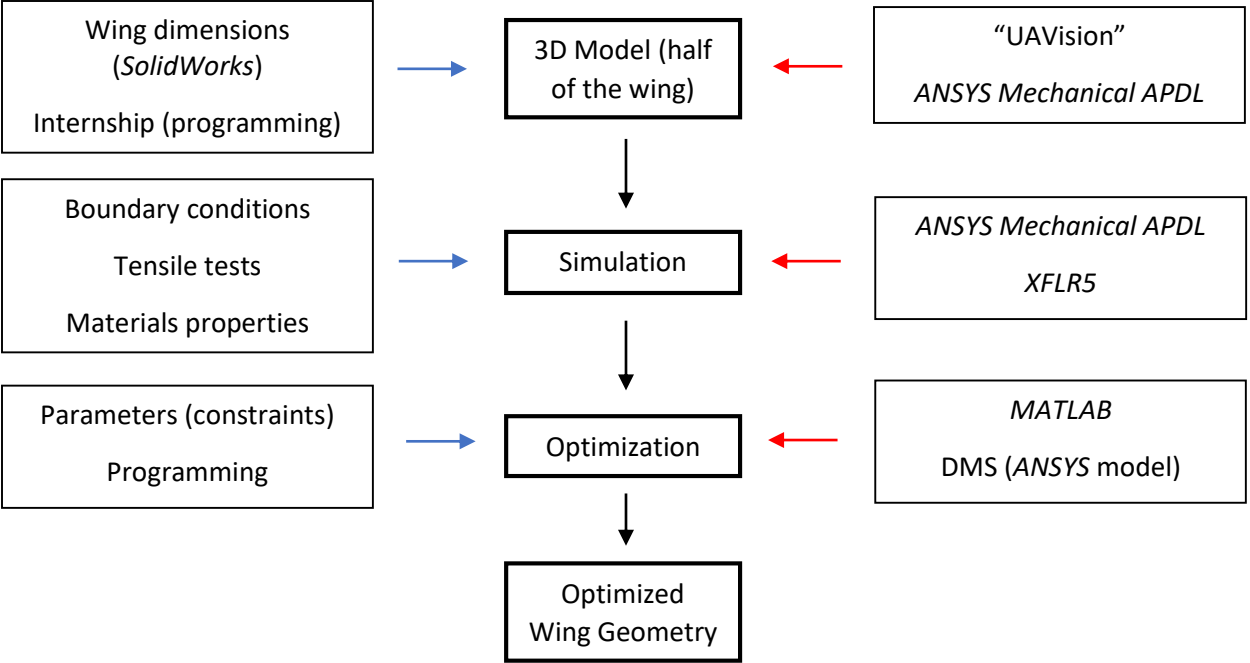


Figure 3 - Work methodology

For the 3D UAV (half) wing *ANSYS* model, besides considering the overall dimensions of the wing (Figure 2), was used the *SolidWorks* model (courtesy of “UAVision”) of it to have the internal reinforcements positions and shapes (ribs, spars and holes). That time was spent in the “UAVision” company, where all the *ANSYS Mechanical APDL* programming process was done. Besides the master’s thesis time, was done a summer internship at “UAVision”.

Using the *ANSYS* model programmed, applying the materials properties and the boundary conditions mentioned in the beginning of this section (*XFLR5*), the structural simulation of the wing (half) was done. For the materials properties, some tensile tests were done in “Técnico Lisboa”, in order to calculate and verify the young’s modulus of the carbon-epoxy composite material used. Besides the carbon-epoxy composite [8], was also defined the “Aluminum 6082 T6” and “Airex C70.75” properties, based on [9] and [10].

The optimization design variables were defined based on the material thickness, quantity of carbon-epoxy laminas applied and on its carbon fiber orientations. Was used the DMS solver in the optimization procedure. As a result of this methodology was achieved an optimal wing geometry.

1.4 Structure of the thesis

Besides the “Introduction”, this document has more 6 chapters:

Chapter 2: The “State of Art”. An overall literature review about composite materials, namely carbon-epoxy. The use of the UAVs nowadays and the concept and definition of the optimization procedure used, DMS. Works related to the present work are mentioned.

Chapter 3: The “Numerical Simulation”. Is described the conceptualization of the *ANSYS Mechanical APDL* model and explained the contribution of the *XFLR5* software to the simulation.

Chapter 4: The “Optimization”. The role of the *MATLAB* is explained. Its interaction with the *ANSYS* program is highlighted. The DMS solver functionality is mentioned.

Chapter 5: The “Results”. A test made in the “UAVision” company of one wing geometry and the numerical results are described, discussed and explained.

Chapter 6: The “Production of the Wing”. The steps from the molds to the final wing structure. The materials used, the tools and some procedures are described.

Chapter 7: The “Conclusions and Future Works”. All the considerations and new features discovered are mentioned. The future work expected to be done by the company is highlighted.

2 State of Art

2.1 Composite Materials

2.1.1 Definition

Composite materials result from the combination of at least two different materials in a macroscopic scale, forming a third one with the best characteristics of its components or even with some characteristics that neither constituent have. Several materials properties can be improved with this approach, not all at the same time, such as the strength, stiffness, corrosion and wear resistance, thermal and acoustical isolation and weight reduction [11] (Figure 4).

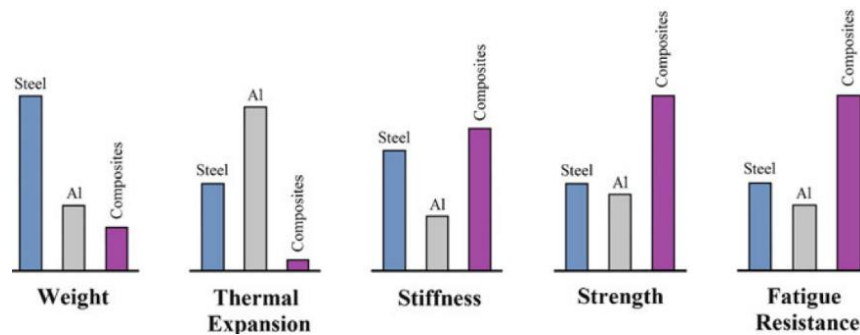


Figure 4 – Qualitative comparison: Composite materials vs monolithic materials [12]

2.1.2 Types of composite materials and their components

Typically, a composite material has three different components: The matrix, the reinforcement and the interface. The matrix plays a key role in the protection of the reinforcement from being exposed to the environmental factors, allows its cohesion and maintains the structural form of the material. While the reinforcement is the principal responsible for bearing the loads, the matrix transfers and distributes them along the reinforcement by shearing stresses (Figure 5). The interface is the “separation phase” between the reinforcement and the matrix [11,13].

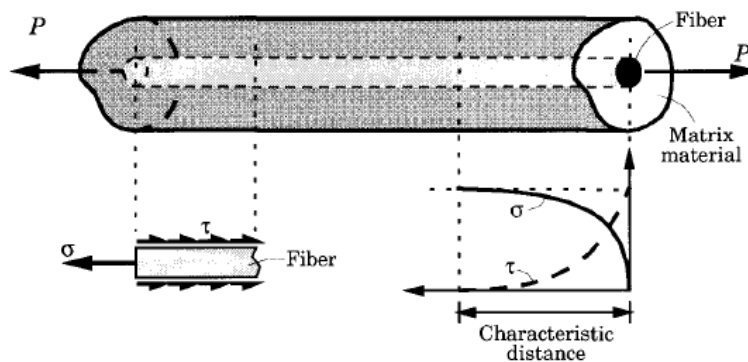


Figure 5 - Load transfer and stress distribution in a composite subjected to an axial load [13]

From the literature [11,13], there are three main types of composite materials:

- Fibrous composite materials (fibers + matrix);
- Particulate composite materials (particles + matrix);
- Laminated composite materials (layers).

The fibrous composite materials are characterized by its stiffness and strength has a consequence of the fibers that compose them. This type of reinforcement has better mechanical properties than bulk materials because of “its very high length-to-diameter ration” and “its near-crystal-sized diameter”. By this way, the fractures are smaller and the defects less than the ones in the bulk materials. The fibers have directionally dependent properties. A whisker is even more perfect than a fiber, in terms of structure, exhibiting higher properties [11,13].

For the particulate composite materials, the particulates and the matrix can be metallic or non-metallic. The size of the reinforcement is smaller than in the fibrous composites [13].

The laminated composite materials are an assembly of laminas or plies (sheet of composite material). The most common way of laminas are the fiber-reinforced ones, where “the fibers can be continuous or discontinuous, woven, unidirectional, bidirectional or randomly distributed” (Figure 6). The unidirectional fiber-reinforced laminas have better properties (highest strength and modulus) in the direction of the fibers than in a transversal direction (directionally dependent properties). The discontinuous fiber-reinforced laminas, when compared to the continuous fiber-reinforced laminas, exhibits a lower strength and modulus. It is important to have a strong bond between the fibers and the matrix material to avoid fiber pull out, fiber breakage and fiber buckling. The orientation of the fibers is important to take into account. Normally fibers orientated at 30° or 45° can take shear loads and at 0° or 90° can take tensile loads [11,13].

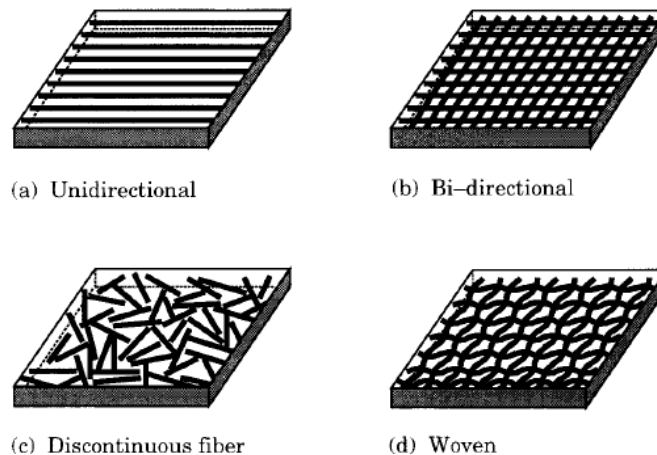


Figure 6 – Some types of fiber-reinforced laminas [13]

2.1.3 Advantages and disadvantages

Besides the fact that the laminated composite materials are used in demanding industries such as in the aeronautic and automobile industries, they have some drawbacks. The main concerned is about a phenome called delamination (separation between the laminas), that can be a caused by mismatch of material properties between layers and the shear stresses produced between them. A similar problem, fiber debonding (separation between the fiber and the matrix), can also occur. Other defects can be introduced during the manufacture of this type of composite materials. “Interlaminar voids, incorrect orientation, damaged fibers and variation in thickness” are some examples of these [11,13].

In Table 1 are listed some advantages and disadvantages of the composite materials.

Table 1 - Advantages vs disadvantages of composite materials [14]

Advantages	Disadvantages
Light weight	High raw materials costs and fabrication costs
Ability to tailor the lay-up for optimum strength and stiffness	Adverse effects of both temperature and moisture
Improved fatigue life	Impact damage
Improved corrosion resistance	Delamination and plies damage
Reduced assembly costs	Difficulties in reparations

Based on [14], one of the major costs in the aeronautic field are due to corrosion problems in aluminum alloys, which are structural materials frequently used. The corrosion resistance of the composite materials results in savings in supportability costs. The use of composite materials simplifies the assembly labor, reducing also the costs associated. However, the industrial techniques to produce composite materials, such as the traditional hand lay-up, requires the need of specialized labor (it can be a complex procedure), increasing the costs. As in all the materials industries, the costs savings are important, namely when 50% of the cost are due to the materials choice and fabrication procedure and 50 % to the fasteners and assembly labour, as it is explained in [14]. Because of that and depending on the application, it is required a balanced and strategic use of composite materials.

2.1.4 Carbon-epoxy composites

Fiber reinforced polymer composites exhibits high mechanical performance levels, comparing them with the traditional metallic materials, due to their stiffness, strength and lightweight characteristics. Those materials are ideal for aircraft components, for the automotive industry, construction and for marine applications [15].

The carbon fibers bear most of the loads and have an important contribution to the composite materials properties. Other advantages like low thermal expansion, durability, corrosion resistance and electrical conductivity characterize those fibers. However, their relative cost and their brittle behavior are two factors that constraint their use [15,16].

The epoxy matrix transfers the loads to the fibers, avoids their degradation and maintain the composite materials cohesive. Besides all these aspects, this resin presents several advantages, as can be read in [17]: Excellent chemical resistance, high adhesion to different substrates, very high tensile, compressive and flexural strengths, excellent electrical insulation properties, corrosion and physical abuse resistance.

It is a common thermosetting polymer used in the structural components of aircrafts, namely as the matrix phase of carbon fibers-reinforced composite materials, because of all the advantages mentioned and the low release of volatiles during curing [18].

As a disadvantage, “most epoxy resins easily ignite when exposed to fire, and release copious amounts of heat, smoke and fumes.”, as is written in [18].

2.1.5 Applications in the aerospace industry

From [19], can be read that “Composite materials are particularly attractive to aviation and aerospace applications because of their exceptional strength and stiffness-to-density ratios and superior physical properties.”

Due to some conflicts such as the Vietnam war, the conflict in Iraq and the cold war, the composite materials suffered several developments. The humid environments, inducing the oxidation and corrosion of the metallic materials, the constant need of weight reduction and better mechanical and electrical properties, were some of the reasons for the increased use of composite materials in the aerospace industry. Low weight structures were and are a core objective in this industry for performance and payload reasons [14,20].

The use of thermoplastic fiber-reinforced composites materials has increased in the aerospace industry, because of their fatigue, impact and heat resistance and their low moisture

absorption. This type of composites has a big versatility to be produced in an industrial scale. When compared with the metallic structures, the thermoplastic based composites represent a weight saving of 25% (average weight saving using composite materials: 15% – 25%), as it is mentioned in [14,20].

There are also the carbon/carbon composite materials, a thermo-structural class that take advantage of the high-performance characteristics from the carbon fibers. The carbon materials have a good mechanical resistance in high temperatures conditions and in the absence of oxygen, high corrosion tolerance, small thermal expansion and they are chemically inert. However, they are brittle and sensitive to imperfections, being its use limited by that [20].

An example of the composite materials application in the aerospace field is the commercial airplane Boeing 787, showed in Figure 7.

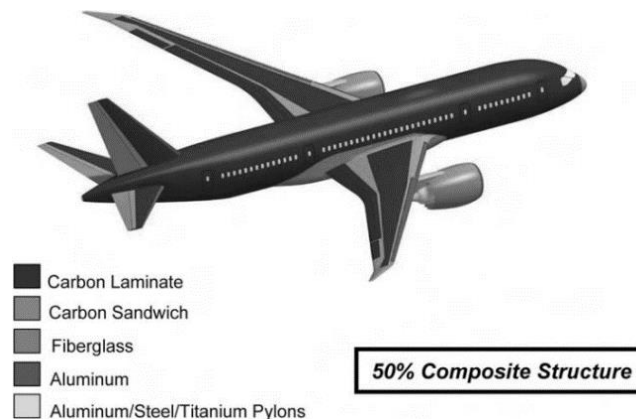


Figure 7 - Boeing 787 structural materials [14]

From the literature [21], other type of composite materials frequently used are the polymer-matrix ones, because of “their relatively low processing costs”. Continuous fiber-reinforced polymer-matrix composites are used for several airplane structural parts, namely in lightweight structures such as airframes. Carbon-epoxy composites (carbon fibers + epoxy matrix) are an example of those, exhibiting advantages in the weight reduction of the structures when compared with metallic structural aerospace materials (Figure 8).

Companies like “UAVision”, use carbon-epoxy composites in the structural components of their UAVs (Figure 9 and Figure 10). In the case of the mentioned company, the carbon-epoxy composite material is bought already in a plate shape, being cut by CNC machines based on their needs. By this way, the manufacture process time is optimized and the number of defects expected from the carbon-epoxy lay-up mechanism is standardized and lower than if it was made in the company.

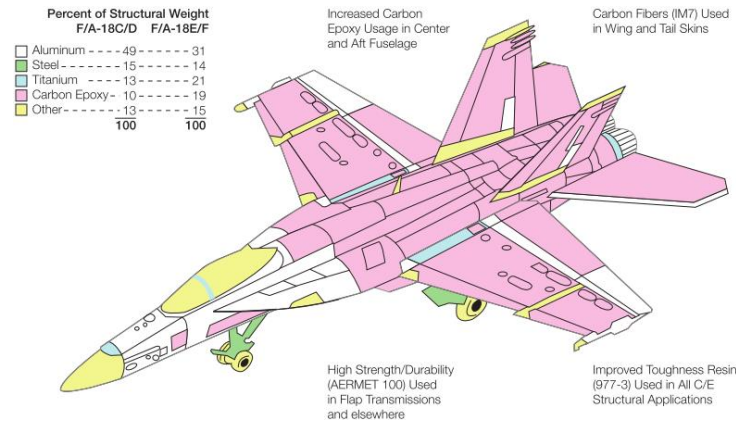


Figure 8 - Structural weight of carbon-epoxy composite vs metals [19]



Figure 9 - Structural components of a UAV wing (courtesy of “UAVision”)



Figure 10 - Carbon-epoxy arm and rotor blades (courtesy of “UAVision”)

2.2 The use of UAVs nowadays

Nowadays the impact of the human being in the environment is visible and it is reaching problematic levels. Maritime accidents, forest fires and emission of pollutant gases, are some examples. In the engineering field is being study and improved some technologies (e.g. the use of UAVs) to avoid, predict and control some of those problems. The UAVs role importance in this type of environments is increasing, showing their versatility and safety advantages, since they can be controlled remotely and provide real time information.

2.2.1 Environmental and rescue missions

Maritime accidents have a direct and long impact in the marine life because of the dangerous oils spilled and the gases and chemicals released. Even simple acts such as the cleaning of shipping containers in the sea as well as their lost, contributes to the environmental devastation [22].

To control and avoid this kind of problems, the UAVs can be used as a surveillance tool as also as a measurement tool, using “air quality monitors (...) aerial imaging systems, radar systems, sonar imaging systems, etc” [22]. All this data can be collected in real-time using transmitters and stored later.

The payloads capacity and their real-time communication characteristics make the use of the UAVs necessary in environmental incidents. Instruments such as: Visible and infrared cameras, radar, chemical sensors, mobile phones detectors and location and environmental sensors can be implemented on the UAVs [23].

Comparing to manned aircrafts, those vehicles are safer and more flexible (control from distant points, can be recoverable (runway, sea surface, parachute or net/hook) and can be launched from anywhere (launching platforms, on land or at sea)) [22].

Forest fires are another example of the advantages of using UAVs (namely fixed wing). In a hot, foggy, smoky and windy conditions is easy to be lost. It frequently happens to fire crews and civils between fire fronts [23].

Because of that, search and rescue (SaR) in forest fires is common and needed. The use of those unmanned vehicles helps in planning and monitoring the operations, facilitating the management of the human and material resources. Due to the use of UAVs is possible to increase the personnel safety by searching over the affected areas and by the air quality monitoring. The main constraints are the strong winds, the high temperatures and the possible failure of the communications (due to the unfavorable conditions and autonomy limitations) [23].

Besides the forest fires, the use of UAVs in SaR can be applied in the sea, mountains and urban areas. Disasters like earthquakes and explosions are some other examples where the use of those vehicles is helpful [23].

Environmental disasters like the forest fires are a real concern for the Portuguese people and government. Because of that, “UAVision” is collaborating with the Portuguese Air Force and the Portuguese military. Using the fixed wing UAVs with cameras and thermic sensors

implemented, some successful tests were already made. By this way, companies like “UAVision” play a key role in our society, applying their technological advancements.

2.2.2 Military applications

From [24], “Military systems are the motivational driver for much of the technology development conducted at applied research laboratories around the world.”

The military needs represent a big engineering challenge. The hostile war environment and the adverse atmospheric conditions take the materials and the mechanisms to their limits. For the new war era that involves military operations in urban terrain (MOUT), the UAVs capabilities are highlighted (“endurance, portability, performance, payload and communication capabilities”), namely in surveillance and reconnaissance operations. Besides the topography, each urban area has different style, construction and density of buildings, being each one a different case study (dynamic environment). The UAVs make possible to have real-time information, helping in the strategy and organization of the military [24].

This type of vehicles has been developed specially for imaging and communication, instead of weaponry. All the logistics involved in the use of the UAVs is simple: Light infrastructure, some laptops and one or two operators [24].

2.2.3 Other applications

The use of UAVs extends to civil applications, such as: Security control (e.g. police, firefighters) traffic and crowd management and agriculture management (Figure 11). The involvement of the UAVs in surveillance activities in those areas can reduce the costs, avoid more serious problems and implement viable management strategies in our cities [25].

However, problems related with privacy and the ethical uses, legislations and licensing are real. Those problems are still being solved by the governments [25].



Figure 11 - A firefighting UAV [25]

2.3 Optimization

2.3.1 Topology optimization

According to [26], “The purpose of topology optimization is to find the optimal lay-out of a structure within a specified region”. Normally, in this kind of optimization approach, it is just known the applied forces, the support conditions, the volume of the structure and some other design constraints (holes, solid areas, etc). In the case of a UAV wing, as the one in study, the external shape of the wing is unchanged, being the position of the internal reinforcements changed (also some holes) as well as the thickness and the quantity of carbon-epoxy laminas used.

Based on [26], there are three categories of structural optimization (Figure 12):

- Sizing optimization;
- Shape optimization;
- Topology optimization.

The biggest difference between the topology optimization and the others two is that the design can attain any shape within the design space. In sizing and shape optimization there are predefined configurations [26].

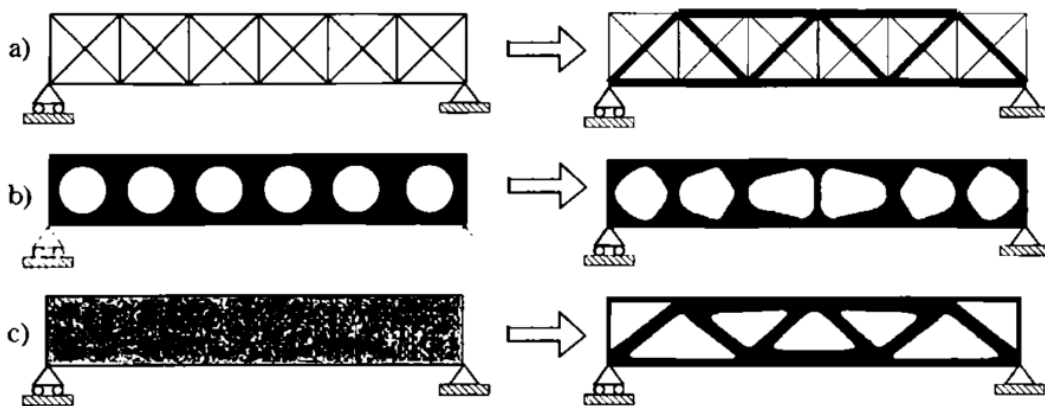


Figure 12 - a) sizing optimization; b) shape optimization; c) topology optimization [26]

Due to the increasing use of composite materials in structures, like in the UAV wing, the optimization of composite structures is needed. The topology optimization is applicable in the material distribution and the orientation of the fibers. This kind of approach is implemented in this work and mentioned in [27], exhibiting an improvement in the performance of composite materials structures.

This technique is currently mostly used at the concept and development phases of the design process. Sometimes the resulting shapes are difficult to be manufactured [27].

2.3.2 Multiobjective optimization

Some important definitions about multiobjective optimization (MOO) will be mentioned and briefly explained in this section.

From [28], a multiobjective problem can be defined as a practical application “where the designer may want to optimize two or more objective functions simultaneously”.

$$\mathbf{x} = (x_1, x_2, \dots, x_n)^T \in \Omega \subseteq \mathbb{R}^n \quad (1)$$

$$\min_{\mathbf{x} \in \Omega} F(\mathbf{x}) = (f_1(\mathbf{x}), f_2(\mathbf{x}), \dots, f_k(\mathbf{x}))^T \quad (2)$$

$$f: \Omega \subseteq \mathbb{R}^n \rightarrow \mathbb{R} \cup \{+\infty\} \quad (3)$$

Subject to

$$h_i(\mathbf{x}) = 0; i = 1 \text{ to } p \quad (4)$$

$$g_j(\mathbf{x}) \leq 0; j = 1 \text{ to } m \quad (5)$$

where k is the number of objective functions, p is the number of equality constraints and m is the number of inequality constraints. \mathbf{x} is a n -dimensional design variables vector, $F(\mathbf{x})$ is a k -dimensional vector of objective functions and Ω the feasible region (the admissible set for the design variables). Note that maximize f_k is the same as minimize $-f_k$.

The “feasible criterion space” (Z), (Figure 13), as is mentioned in [28], “is simply a set of objective function values corresponding to the feasible points in the design space”.

$$Z = \{F(\mathbf{x}) | \mathbf{x} \text{ in the feasible set } \Omega\} \quad (6)$$

Looking to the two solutions, A and B in Figure 13, is visible that solution A has a smaller z_1 value but a higher value of z_m , comparing it to the values of solution B. When it happens, none of these solutions can be considered better than the other with respect to both objective functions values. These solutions are considered as nondominated solutions [30].

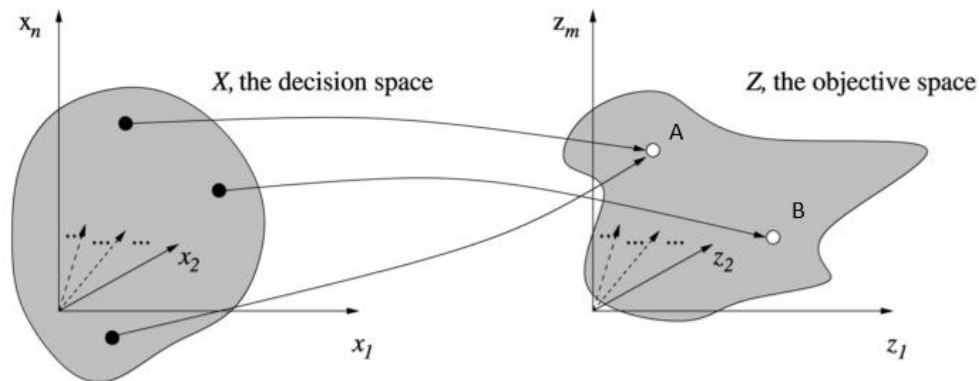


Figure 13 - Feasible criterion space [29]

The “Pareto optimality” is the concept of solution in a MOO problem. “The *Pareto optimal* set X^* of solutions consists of all those that it is impossible to improve in any objective without a simultaneous worsening in some other objective”, as it is mentioned in [29].

Figure 14 illustrates the Pareto optimal set for four different objective functions hypotheses. Depending on if it is maximizing or minimizing the objective functions of a certain problem, the Pareto optimal set solutions has different locations. In the present work, once there are two objective functions being minimized, is expected to obtain an approximation to the Pareto optimal set solution like the one of the top left corner image, in Figure 14 [30].

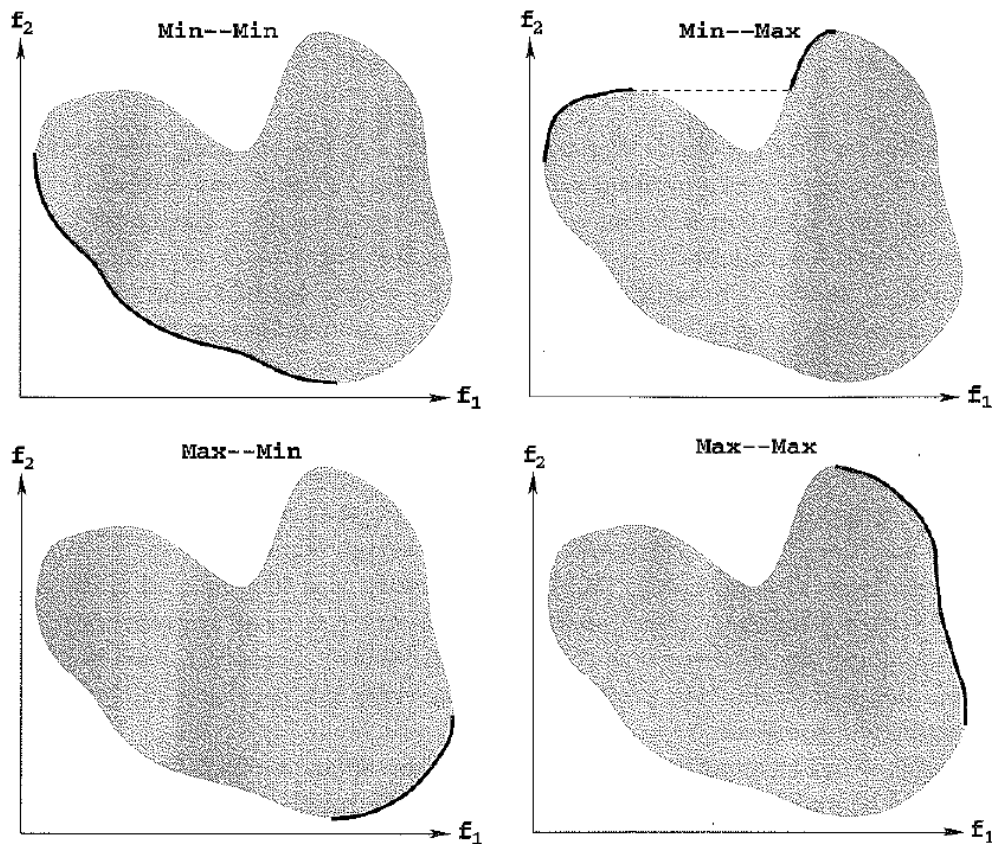


Figure 14 - Pareto front for 4 different objective functions combinations [30]

Based on what is written in [28], the term “weak Pareto optimality” appears when “it is possible to improve some objective functions without penalizing others”. The same cannot happen in the Pareto optimal points, improving an objective function without prejudice others.

In the MOO problems, there are no single solutions. In the Pareto front region, there are several points (Pareto optimal points) that represent all the possible solutions. Depending on the

problem and its constraints, the engineers are the ones who choose the best solution of the problem in question. The MOO approach helps them to understand the resolutions for the conflicting objectives [31].

One of the objectives using MOO is to find the maximum different Pareto-optimal solutions as possible. The Pareto front can be convex, non-convex, continuous and discontinuous. In the case of the discontinuous Pareto fronts, some of the sub-regions can be discarded when compared with others, due to the constraints of the problem [32].

It is also frequent to have a not uniformly distributed Pareto-front, where there are some regions with a higher density of points [32].

2.3.3 Direct Multisearch (DMS)

The authors in [7] presented a new multiobjective derivative-free methodology, the “direct multisearch” (DMS), which does not aggregate any of the objective functions. This method is based on a search step and a poll step. It uses the Pareto dominance concept, maintaining a list of feasible points (the best approximation to the Pareto front), nondominated points, from where the new poll centers are chosen. Every iteration new nondominated points are added to this list, while the dominated ones are removed. When this list of feasible points changes, the iteration is considered as successful. When it doesn't, the iteration is considered as unsuccessful. The purpose of this method is to create the biggest amount of points in the Pareto front as possible, from the polling procedure.

The local search step occurs around a poll center, testing different directions scaled by a step size parameter. When an iteration is considered as successful, the step size parameter is maintained or increased, while in unsuccessful iterations it is decreased [7, 33].

Being the feasible region represented by Ω , it is used the following barrier approach:

$$f_{\Omega}(\mathbf{x}) = \begin{cases} f(\mathbf{x}) & \text{if } \mathbf{x} \in \Omega \\ (+\infty, \dots, +\infty)^T & \text{otherwise} \end{cases} \quad (7)$$

Which means that the components of the objective function of an infeasible point are not evaluated, allowing to deal with black box-type constraints [7].

There are different ways to generate the initial list of points (DMS variants), explained in the “chapter 6” of [7]. In the present work was used the “DMS (n, rand)”.

For a complete interpretation of the DMS solver is recommendable to read [7, 33].

2.4 Previous optimization works

In [34], was done a multiobjective approach optimization to reduce the vibration in sandwich structures, using the DMS solver. The goal was to maximize damping while minimizing weight, in sandwich plate structures. The design variables are the layer thickness, layer material and the orientation angles of the laminate layer ply. A comparison between the results obtained using the DMS solver and some genetic optimization algorithms was made. In that work is described the finite element model of the sandwich (viscoelastic core, laminated anisotropic face layers, top and bottom piezoelectric sensor and actuator layers), the DMS solver, the optimal design formulation and three applications (simply supported sandwich beam; simply supported sandwich plate; simply supported sandwich plate with viscoelastic core and material design variables). The results from the DMS, comparing it with the ones obtained by genetic algorithm, were classified as “more reliable solutions”. The importance of the Pareto front is also fomented and is concluded that “DMS provides more and better solutions for most cases”.

The work in [34] proves the functionality of the DMS optimization solver when compared to others, namely when applied to composite structures. That work shares the goal of weight minimization of a composite structure, some optimization parameters and the optimization solver method, when comparing it with the present work.

In [35], was studied and optimized the mechanical behavior of a composite structure (spar approximation) used in unmanned platforms. The goal was to minimize the maximum deformation of that structural component (when subjected to a specific load), based on a uni-objective direct search method, GLODS. Was considered a fixed amount of laminas with variable orientation values. This optimization procedure was ensured by an interaction between the ANSYS software and the GLODS solver. Were produced some specimens and some bending tests were performed. An innovation method was used to measure the strain results, the “digital image correlation”. Was used the ANSYS software in the numerical simulation step as well as a new computational method, the “layerwise”. The results from the experimental tests and the ones from the numerical simulations were compared. Was concluded that the results from ANSYS were closer to the experimental ones for longer specimens, while the results from the “layerwise” method were closer to the ones related to the shorter specimens. A 50% decrease on the maximum deflection was achieved with the optimized specimens.

Based on [35] is also possible to identify some common aspects with the present work: The interaction between the FEM software and the optimization solver, the study of a composite

structure and the minimization of the maximum deflection value of the structure. Besides being a uni-objective problem, the optimization solver used is also a direct search method.

In [36], was optimized the structure of a UAS (class I 145 kg) wing. The design and optimization process involved the determination of the forces applied on the wing, the wing geometry, the location of the components and the choice of the materials. Was used the *SolidWorks* software for the 3D modelling. An optimization of the structural components was done, ensuring the minimum value of mass and costs. The structural analysis was ensured by a structural FEA (Finite Elements Analysis) and was used a 4 step “chain top-down” optimization process. It is inspired by the topology optimization method logic (for better understanding, read [36]).

This work is focused more on the wing components design, reaching an almost 3000 € wing configuration, based on the materials and the manufacture process costs. In this work is highlighted the FEA and the use of composite materials, in a topology wing based optimization.

In [37], was made a multiobjective design optimization of laminated composite plates with piezoelectric layers. Different behavior constraints were considered, for example the maximization of buckling load, weight minimization and the minimization of the electric voltages applied in the piezoelectric actuators. Stress based failure criteria and other structural response constraints restricted the optimization problems. The design variables were the fiber orientations in the composite layers, its thickness and the electric potentials applied to the actuators. Once this problem is a multiobjective one (“k objectives”), the local extremes values of the objective functions were assumed as “k single-objective” optimization problems, being solved using GLODS. From that approach, the multiobjective algorithm is initialized and was used the DMS solver. Both solvers are explained in [37]. There were two applications: “Optimal fiber orientations in a composite plate with piezoelectric layers” and “Optimal design of a cantilever piezoelectric actuator/substrate plate”. Was obtained a considerable number of nondominated solutions, namely a weight reduction of 40% with respect to the initial design, in the second application.

The [37] work is another example of a composite structure multiobjective optimization, where the DMS solver is used. It has some design variables and the weight minimization goal in common with the present work.

In [38] was done a dynamic analysis and design of impact attenuator structures for a formula students prototype, testing its performance. A FEM was used in order to do some performance simulations of the structure. The goal is to analyze, design, manufacture and test

different solutions of that structure. Possible solutions were simulated and tested, namely using aluminum tubes and carbon fiber tubes. The nose of the formula student car (one of the impact structure parts), was analyzed and optimized, using DMS, a MOO approach that consists in minimizing both mass and impact maximum acceleration of the nose simultaneously. Was achieved a weight saving of 68% (of the composite nose structure).

The work developed in [38] is another work in the structural analysis field, analysing composite materials, using the DMS solver in the optimization procedure. Besides being a car component analyzed, this work shares some approaches with the one described in this document, namely the optimization solver used.

In [39] was done an optimization, computational and experimental studies of hybrid laminated composite specimens, analyzing their performance when subjected to deflection and torsional loads. The composite structures were based on epoxy matrix reinforced by carbon and glass fibre laminas (hand lay-up). Was used the *ANSYS* software (*Workbench*) in the computational simulation, comparing its results with the experimental ones. For the optimization process, was used the solver *GLODS* (interaction with *ANSYS Mechanical APDL*). The optimization goal was to minimize the maximum displacement verified on the structure. The influence of the position and fiber orientation of the laminas in the results were considered. With this work were achieved different optimized laminated sequences for the specimens in study, reaching a decrease of 30% and 76% in the maximum displacement values.

The work in [39], like the others that have been mentioned in this section, corresponds to other example of structural analysis and optimization of a composite structure. The *ANSYS* software is one more time used.

In [40] the work is focused on the construction and analysis of a lightweight fixed-wing UAV prototype. Was used the *CATIA* software to do a 3D model of the wing. The materials selected (e.g. fiberglass composite) were tested and validated using the *CATIA* model and their elastic properties were calculated. The construction of the wing was described. Was also done a FEA, being the results compared with the experimental ones. Was achieved a new wing design, being the main goal of this work the production of that prototype and obtain a numerical model to predict its behavior.

This work in [40] shares the fact that the component in study is a fixed UAV wing. Was also built a 3D model of the wing and done a FEA. Besides having different goals ([40] and the present work), the structural behavior of the prototype was taken into account.

In [41] is presented an optimal design of a UAV wing constituted by composite materials. The goals of the optimization process were the reduction of mass while improving the stiffness and strength of the structure (mechanical properties of the wing). Was implemented the evolutionary multiobjective algorithm in the optimization of the UAV wing. The design variables of this problem are 24 in total. Was created a FEM model, considering different composite materials (combination of carbon and glass fabric with polyurethane foam), based on the real wing structure. Some tests were performed (tensile and bending tests), validating the FEM model (comparing the experimental results with the numerical ones). Some multiobjective examples using the Pareto optimal set of solutions are mentioned in this work. Was achieved a reduction of almost 27% in the total mass of the structure, while in terms of maximum stresses was achieved a reduction over 50%, for the same level of mass of the structure.

The work in [41] gets close to the current one in several aspects. It is a multiobjective optimization work, where the component in study is a UAV wing. Was done a FEM model, some experimental tests and for the optimization process were considered 24 design variables. One of the optimization goals is also the minimization of the structure weight and was considered the concept of Pareto optimal set of solutions.

All the works mentioned in this section, somehow, share aspects with the present work being described in this document. The main common aspects are the optimization processes, the materials used, the structural components in study and the FEM models and FEA done. However, the present work is distinguished by the fact that it is done in collaboration with a Portuguese company, "UAVision", being expected to implement the optimization improvements in the real UAV wing and manufacture it later. This fact enabled a contact with the company routines, being possible to have a real notion about part of the aeronautic industry in Portugal. The wing in study was not a prototype or a composite specimen, but a full scale fixed UAV wing that is currently being used by the company. All the optimization objective functions and design variables defined in this work are a consequence of the company needs. Also the materials used are the ones that the company apply on their wings.

3 Numerical Simulation

3.1 ANSYS Mechanical APDL model

3.1.1 Introduction

The topology optimization required the elaboration of a parametrized wing model. It was the most efficient approach, in terms of the engineering needs and goals, to simulate and optimize the structure of the UAV wing. As a consequence of that, was chosen the software ANSYS, namely the *Mechanical APDL* interface. A “bottom-up” strategy based programming was built from scratch to achieve the 3D wing model.

3.1.2 Conceptualization of the model

Since the wing is symmetric, it was modelled just half. A few geometrical approximations were done, due to time restrictions, namely the connection with the tail boom. Also the real wing is divided in two (for an easier transportation of the UAV), while the approximated model (ANSYS) is a “one-piece wing”. Comparing the Figure 15 with Figure 16, these approximations are visible.

The following steps represent the reasoning behind the programming process:

1. Define:
 - a. Type of analysis: Structural linear static;
 - b. Finite element type: SHELL181 (4 nodes elements, 6 DoF per node)
 - c. The materials: Carbon-epoxy, “Aluminum 6082 T6” and “Airex C70.75”
2. Define the geometry:
 - a. Create key points;
 - b. Unite the key points by lines;
 - c. Fulfil the gaps delimited by the lines, forming areas;
 - d. Sum and subtract areas (to make holes).
3. Define and apply the mesh;
 - a. No. of nodes: 103075
 - b. No. of elements: 103862
4. Apply the boundary conditions;
5. Solve
6. Output:
 - a. Maximum deflection of the wing;
 - b. Mass value of the wing.

The geometry was modelled respecting the external wing dimensions (Figure 1, section 1.1)). Based on the “airfoil NFL – 416”, the ribs were defined. After that, they were united by areas along the wing (forming the exterior “skin”), and the winglet was modelled. The following parts were the spars and the holes. By that way, the basic structure of the wing was replicated. In Figure 17 is demonstrated the interior of the wing, exhibiting the internal reinforcements and the holes.

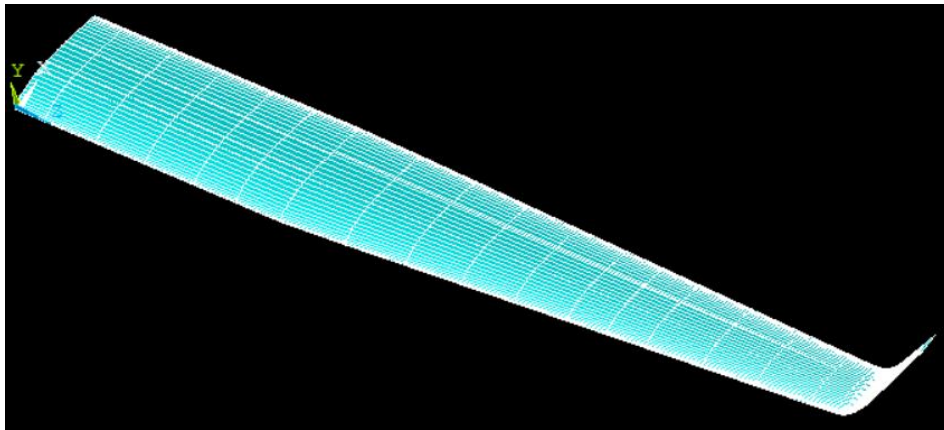


Figure 15 - 3D wing model (ANSYS model)



Figure 16 - UAV wing (courtesy of “UAVision”)

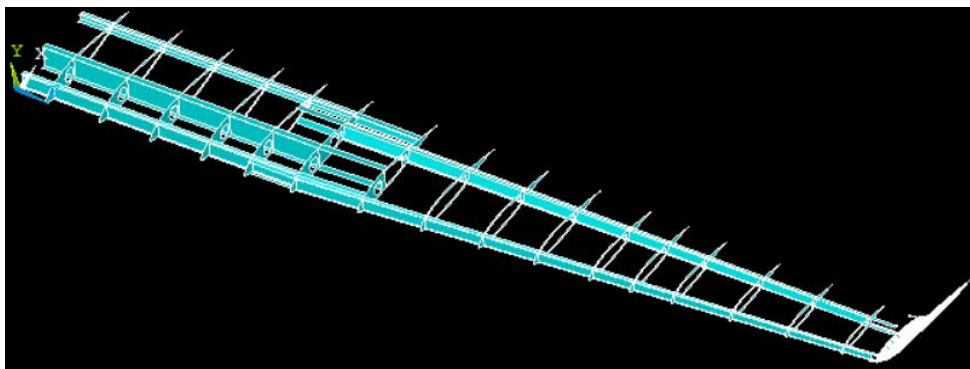


Figure 17 - Interior of the 3D wing model (ANSYS model)

3.1.3 Mesh and boundary conditions

It is important to design the most regular and constant mesh as possible. It is a critical step that will influence directly the quality of the results obtained from the simulation method.

Considering that the internal reinforcements (spars) and the holes of the wing change their position during the optimization process (parametrized model), the mesh was created instead of being randomly generated. Through the key points, the lines associated were identified and measured. Having that information, the lines were divided according to their size to maintain always the same number of divisions per section of line. By this way, even with the interior reinforcements and holes moving, the standardization of the mesh was ensured. As a consequence of that strategy, the mesh adapts to the moving parts of the wing. In Figure 18 and Figure 19 is possible to visualize the lines and part of the mesh, correspondently.

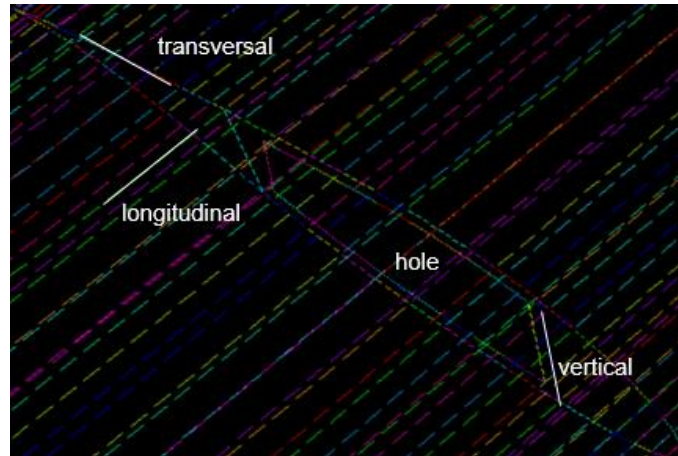


Figure 18 - Division of the lines to generate the mesh (ANSYS model)

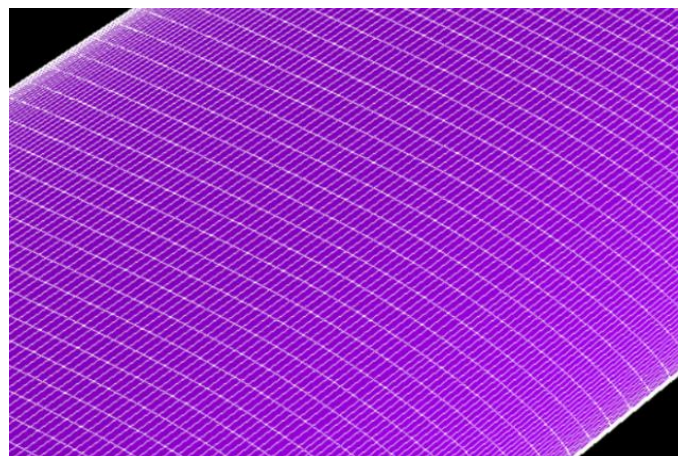


Figure 19 - Mesh (ANSYS model)

Was tested and then assumed an acceptable number of line divisions considering its length (Figure 18):

- No. divisions per vertical line: 10;
- No. divisions per longitudinal line: 15;
- No. divisions per transversal line: 15;
- No. divisions per line (hole): 10.

in order to achieve the most constant mesh as possible. It was the best approach to a refined mesh, due to restrictions of time.

Regarding the boundary conditions, was used the *XFLR5* software to simulate the loads that the wing must bear during stationary flight conditions. A 3D wing was modelled using that software (Figure 20) and an aerodynamic analysis was done. The obtained distributed loads profile was applied on the key points of the ribs along the wing (Figure 21), in the *ANSYS* model.

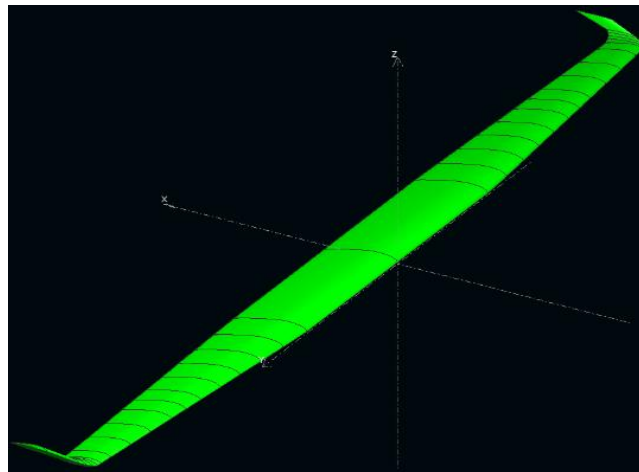


Figure 20 - 3D wing model (*XFLR5*)

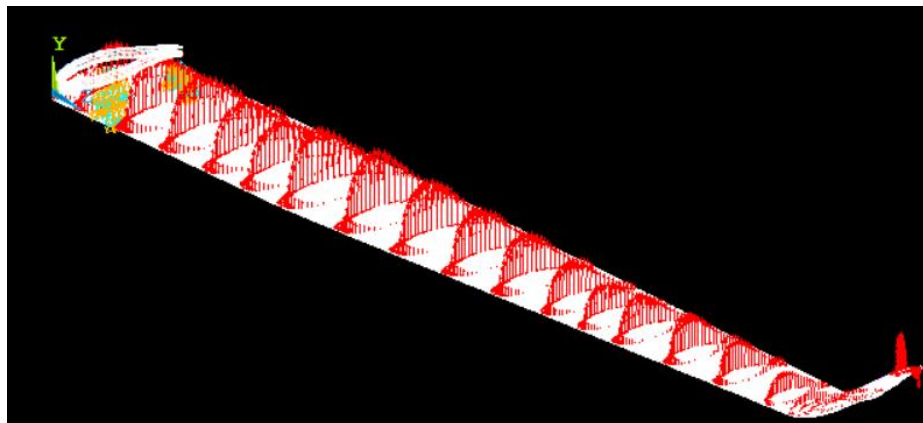


Figure 21 - Loads from *XFLR* applied on the wing (*ANSYS* model)

Besides that, since it was modelled half of the wing in the *ANSYS*, in the tip opposing the winglet was applied a fixed end boundary condition (just in certain key points (in the aluminum rib), simulating the carbon tubes used in the real wing). Finally, a symmetry boundary condition was applied on the same tip, but on the key points of the “exterior skin”, since the wing is symmetric. In Figure 22 is showed these boundary conditions (yellow – fixed end; white – symmetry).

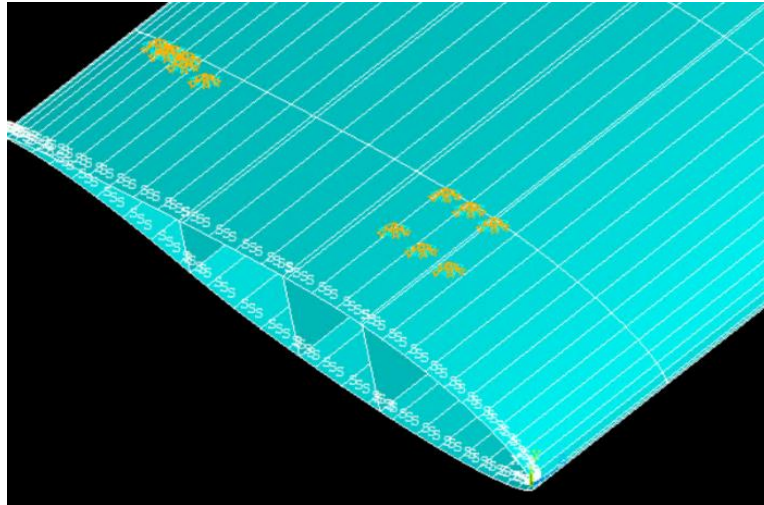


Figure 22 - Symmetry and fixed end boundary conditions (*ANSYS* model)

3.1.4 Materials

The materials used in the wing manufacture are:

- Carbon – epoxy composite material
- “Airex C70.75” (core material)
- “Aluminum 6082 T6”

In order to verify and calculate some of the mechanical properties of the carbon-epoxy composite material, since it is the major material used in the wing manufacture, some tensile tests were done.

Tensile Tests

Carbon-epoxy specimens

The carbon-epoxy specimens were provided by the “UAVision” company. As can be seen in Figure 23 and Figure 24, it was obtained using a CNC machine (Haas VF-4SS) by cutting a

sheet of 2x2 twill weave carbon fiber pattern (epoxy matrix). It has 8 laminas of carbon: 90° oriented laminas (4) and 0° oriented laminas (4).



Figure 23 - Sheet of 2x2 twill weave carbon fibre (courtesy of “UAVision”)



Figure 24 - Haas VF-4SS used to cut the specimens (courtesy of “UAVision”)

Were used two types of carbon-epoxy specimens (three of each type):

- epoxy + bi carbon fibre 0°/90°
- epoxy + bi carbon fibre +45°/-45°

In the Table 2, are expressed the dimensions of the specimens. The choice of the length and the width dimensions was based on [36]. The thickness was based on the material available.

Table 2 - Dimensions of the Specimens [36]

Length [mm]	250
Width [mm]	25
Thickness [mm]	1.6

Experimental procedure

The goal of the tensile tests was to obtain the real young's modulus value, in the direction of the applied tensile load, of the carbon-epoxy composite material used in the wing. The experimental procedure was carried out in accordance with the regulations from the "American Society for Testing Materials (ASTM)", namely the D3039/D3039M.

To have the most consistent results, all the six specimens were obtained from the same sheet of carbon-epoxy composite material (Figure 23).

During the tensile tests, was used an extensometer, "INSTRON 2630-106" (Figure 25), a unidirectional strain gage. It is characterized by its speed of attachment (clip-on extensometer) and its error prove details. Some of its specifications are showed in the Table 3.



Figure 25 - INSTRON 2630-106 (courtesy of "IST")

Table 3 - INSTRON 2630-106 specifications [42]

Gauge Length [mm]	25
Specimen Diameter [mm]	20
Specimen Thickness [mm]	0 – 12.5
Specimen Width [mm]	0 – 40
% Travel (axial)	+50/–10%

The testing machine used in the tensile tests was the "INSTRON 5566" (Figure 26), with a 10 *KN* load cell. The rate of the tensile test was 5 *mm/min* and the temperature was around 21 °C (room temperature).

The data obtained directly from the software associated to the extensometer and the tensile test machine was, for each specimen an excel document with the values of displacement, strain, load and tensile stresses, like the one in Figure 27.



Figure 26 - INSTRON 5566 (courtesy of “Técnico Lisboa”)

Time (sec)	Extension (mm)	Load (N)	Tensile strain (mm/mm)	Tensile stress (MPa)	Strain 1 (mm/mm)
0	0	-9.72	0.00001	-0.26	0.00001
0.1	0.0072	20.48	0.00002	0.55	0.00002
0.2	0.01649	101.36	0.00006	2.7	0.00006
0.3	0.02488	164.2	0.00009	4.38	0.00009
0.4	0.03321	222.98	0.00012	5.95	0.00012
0.5	0.04154	278.41	0.00015	7.42	0.00015
0.6	0.04998	332.4	0.00017	8.86	0.00017
0.7	0.05831	383.7	0.00019	10.23	0.00019
0.8	0.0667	431.63	0.00021	11.51	0.00021
0.9	0.07497	475.83	0.00022	12.69	0.00022
1	0.08319	515.95	0.00023	13.76	0.00023
1.1	0.09157	551.91	0.00024	14.72	0.00024
1.2	0.0999	583.32	0.00024	15.56	0.00024
1.3	0.10835	609.92	0.00025	16.26	0.00025
1.4	0.11673	632.71	0.00025	16.87	0.00025
1.5	0.12506	651.32	0.00025	17.37	0.00025
1.6	0.13328	666.42	0.00026	17.77	0.00026
1.7	0.14155	679.95	0.00026	18.13	0.00026
1.8	0.14983	692.38	0.00027	18.46	0.00027
1.9	0.15833	704.72	0.00027	18.79	0.00027
2	0.16671	716.02	0.00027	19.09	0.00027
2.1	0.17516	727.61	0.00027	19.4	0.00027
2.2	0.18337	739.28	0.00028	19.71	0.00028
2.3	0.19159	750.75	0.00028	20.02	0.00028
2.4	0.19998	760.23	0.00029	20.27	0.00029

Figure 27 - Experimental data example

The “epoxy + bi carbon fiber 0°/90°” demonstrated a better mechanical behavior than the “epoxy + bi carbon fiber +45°/-45°”, which didn’t bear the load applied. The “+45°/-45°” ones showed an ultimate tensile stress around 100 MPa. As mentioned in the “section 2.1.2”, the fibers orientated at 45° bear shear loads better and at 0° or 90° bear tensile loads better.

In the Figure 28 are exhibit the specimens after the tensile test. The “epoxy + bi carbon fibre 0°/90°” are the no. 1, 2, 3 and the “epoxy + bi carbon fibre +45°/-45°” are the no. 4, 5, 6.



Figure 28 - Carbo-epoxy specimens after the tensile test (courtesy of “Técnico Lisboa”)

3.1.3 Young’s modulus calculation

Analysing the data obtained, was possible to calculate the young’s modulus, in the direction of the applied tensile load of the carbon-epoxy composite material. The young’s modulus can be calculated using the Equation 8.

$$E = \frac{\sigma}{\epsilon} \quad (8)$$

where E corresponds to the young’s modulus, σ to the tensile stress and ϵ to the strain.

Having the values of the tensile loads from the data obtained, the tensile stress can be obtained using the Equation 9.

$$\sigma = \frac{F}{A} \quad (9)$$

where F is the tensile load applied and A the initial cross section area of each specimen.

Since the young's modulus is the slope of a stress-strain graphic (elastic domain), and having the load-strain data, was chosen two points from the most constant part and calculated the correspondent stress values. Having the stress and the strain values of those points, the young's modulus of each specimen was obtained using Equation 10. To reach the final values of the young's modulus, was made an average of the young's modulus values from each specimen. The values can be seen in Table 4 and Table 5. It was assumed that the average values of the young modulus are the same in the x, y, z directions (an approximation forced by the test and tools limitations). Comparing that values with the ones from the suppliers [8], they are lower. Systematic errors and normal manufacture imperfections contribute for that difference.

$$\text{slope} = E = \frac{\sigma_2 - \sigma_1}{\epsilon_2 - \epsilon_1} \quad (10)$$

Table 4 – Values of the calculations to obtain the young modulus

Specimen	A [mm ²]	F ₁ [N]	F ₂ [N]	ε ₁ [mm/mm]	ε ₂ [mm/mm]	σ ₁ [MPa]	σ ₂ [MPa]
1 (0°/90°)	40	2068.6	3113.3	0.00075	0.00115	51.71	77.83
2 (0°/90°)	40	2078.7	3124.8	0.01876	0.01918	51.96	78.12
3 (0°/90°)	40	2071.9	3123.9	0.00997	0.01041	51.79	78.09
4 (±45°)	40	1626.8	2110.7	0.00237	0.00332	40.67	52.76
5 (±45°)	40	1630.4	2114.2	0.01391	0.01487	40.76	52.85
6 (±45°)	40	1631.3	2110.8	0.01401	0.01306	40.78	52.77

Table 5 – Young's modulus values

Specimen	E _i [GPa]	E _{average} [GPa]	E _{suppliers} [GPa]
1 (0°/90°)	65.3	62.46	70
2 (0°/90°)	62.3		
3 (0°/90°)	59.8		
4 (±45°)	12.7	12.63	17
5 (±45°)	12.6		
6 (±45°)	12.6		

The carbo-epoxy composite material is the most used one, due to its mechanical characteristics (explained in section 2.1.4)). It constitutes the exterior skin of the wing and the reinforcement parts (ribs and spars) of it. Some of its properties defined in the *ANSYS Mechanical APDL* model are in Table 6.

The “Airex C70.75” makes the core of the carbon-epoxy laminas. It is a low density material (cross-linked polymer foam) that combines stiffness and strength to weight ratios with superior toughness. It has a good impact and fatigue strength, having several applications,

namely in the fuselage and wing of aircrafts. Some of its characteristics defined in the *Ansys Mechanical APDL* model are in Table 7 [9].

Table 6 - Carbon - epoxy properties [8]

$0^\circ \setminus 90^\circ$	
Young's Modulus $0^\circ (E_1)$	62.46 GPa
Young's Modulus $90^\circ (E_2)$	62.46 GPa
Major Poisson's Ratio (ν_{12})	0.1
Shear Modulus (G_{12})	5 GPa
Density (ρ)	1600 kg/m ³
$\pm 45^\circ$	
Longitudinal Young's Modulus (E_1)	12.63 GPa
Transversal Young's Modulus (E_2)	12.63 GPa
Poisson's Ratio (ν_{12})	0.77
Shear Modulus (G_{12})	33 GPa
Density (ρ)	1600 kg/m ³

Table 7 - Airex C70.75 properties [9]

<i>Airex C70.75</i>	
Young's Modulus (E_1)	66 MPa
Poisson's Ratio (ν_{12})	0.1
Density (ρ)	80 kg/m ³

The "Aluminum 6082 T6" is a medium strength alloy with excellent corrosion resistance. It is known as a structural alloy. Some of its properties defined in the *ANSYS Mechanical APDL* model are in Table 8 [10].

Table 8 - Aluminum 6082 T6 properties [10]

<i>Aluminum 6082 T6</i>	
Young's Modulus (E_1)	70 GPa
Poisson's Ratio (ν_{12})	0.3
Density (ρ)	2700 kg/m ³

The carbon-epoxy composite materials are considered as orthotropic, while the “Airex C70.75” and the “Aluminum 6082 T6” are isotropic. In the case of the orthotropic materials, there are nine independent elastic constants ($3 E's, 3 \nu's, 3 G's$). Their properties are different in the three orthogonal directions. Once the tensile test was limited to the axial direction, the missing values of the young’s modulus, poisson’s ratio and shear modulus from the Table 6, were considered the same as the ones exhibited. This type of approximation can be assumed because it is considered that the amount of 0° carbon fibres in the specimen is the same as the quantity of 90° carbon fibers. The same happens with the $\pm 45^\circ$ carbon fibers. In the case of the isotropic materials, the properties are all the same in all the directions. By that way, it is just needed two elastic constants to define them (E and ν) [43].

3.1.4 Output

The output values are written in a “.txt file” as can be seen in Figure 29. When the wing geometry is valid appears two values (maximum deflection (m) of the wing and its mass (kg)), when it is not, appears ∞ in both lines (explained in “section 2.3.3”), instead.

The maximum deflection of the wing corresponds to the value measured in the node located in the winglet tip (red point in Figure 30). The mass value is calculated by the ANSYS model, using the function “*GET” selecting all the elements of the wing.

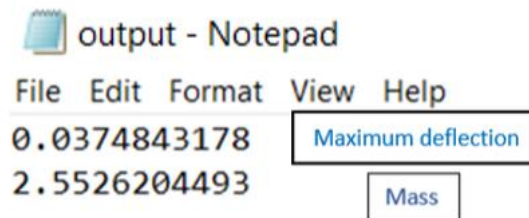


Figure 29 - Output ".txt" file

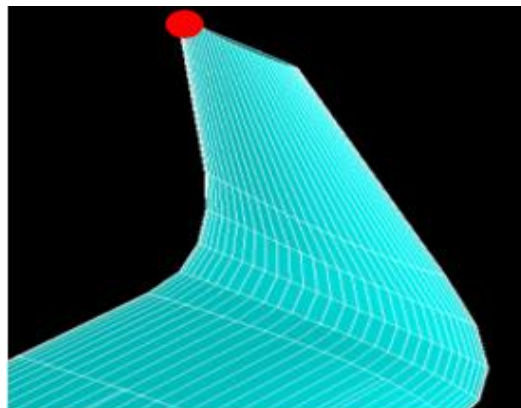


Figure 30 - Winglet tip where the maximum deflection is measured (ANSYS model)

4 Optimization

4.1 Introduction

The optimization process, using the DMS solver, is implemented using *MATLAB*. Was needed to code and edit some scripts to ensure the interaction with the *ANSYS Mechanical APDL* model.

The goal is to find the nondominated points that minimize the two objective functions at the same time, which are: The maximum deflection value of the wing ($f_1(x)$) and its mass value ($f_2(x)$). The mass value represents the principal objective function to be optimized. The maximum deflection value, due to some of the geometrical approximations done (mentioned in “section 3.1.2”), is expected to be lower than the one from the real wing.

Based on that, it is possible to formulate the problem in the following way (Equation 11, Equation 12 and Table 9):

$$\min_{x \in \Omega} F(x) = (f_1(x), f_2(x))^T \quad (11)$$

Subjected to:

$$x = [x_1, \dots, x_{24}]^T \in \Omega \subseteq IR^n \quad (12)$$

Table 9 - Optimization design variables x_i

x_i	Value	Variable description
x_1	{10, 15, 20, 25, 30}	x position % of the spar 1
x_2	{35, 40, 45}	x position % of the spar 2
x_3	{65, 70, 75, 80}	x position % of the spar 3
x_4	{7, 14, 21, 28, 35, 42}	x position % of the spar 4
x_5	{2, 3, 4, 5}	No. of laminas in the exterior skin
x_6	{1, 2}*	Carbon fibers orientation in the exterior skin
$x_7, x_{10}, x_{13}, x_{16}, x_{19}$	{2, 3, 4, 5}	No. of laminas in spar $i = 1$ to 5
$x_8, x_{11}, x_{14}, x_{17}, x_{20}$	{0, 4, 8, 12, 16}	Core thickness in spar $i = 1$ to 5 (mm)
$x_9, x_{12}, x_{15}, x_{18}, x_{21}$	{1, 2}*	Carbon fibers orientation in spar $i = 1$ to 5
x_{22}	{2, 3, 4, 5}	No. of laminas in rib $i = 2$ to 16
x_{23}	{0, 4, 8, 12, 16}	Core thickness in rib $i = 2$ to 16 (mm)
x_{24}	{1, 2}*	Carbon fibers orientation in rib $i = 2$ to 16

In Table 9, the $\{1,2\}^*$ means: $1 \rightarrow 0^\circ \setminus 90^\circ$ or $2 \rightarrow \pm 45^\circ$. The first four design variables (x_1 to x_4) corresponds to the “ x position %” of the four mobile wing spars. It is measured from the leading edge of the wing, 0%, to the trailing edge, 100% (illustrated in the “section 4.2”). The variables x_5 and x_6 correspond to the materials characteristics (no. of carbon-epoxy laminas and its carbon fibers orientation) of the exterior wing skin. The variables x_7 to x_{21} , are the materials characteristics of the five wing spars (no. of carbon-epoxy laminas, the thickness (mm) of the core material (“Airex C70.75”) and the orientation of the carbon fibers). The variables x_{22} , x_{23} and x_{24} are the material characteristics of the fifteen wing ribs (no. of carbon-epoxy laminas, thickness (mm) of the core material (“Airex C70.75”) and orientation of the carbon fibers). The design variables are explained in more detail and illustrated in “section 4.2”.

The rib 1 is constituted by “Aluminum 6082 T6”, with a fixed 10 mm thickness and the spar 5 is fixed (x position). Because of that, these parameters are not design variables. Was considered a symmetrical lay-up (e_1 is symmetric to e_2), which means that the real number of the laminas is twice the values of the design variable (Figure 31).

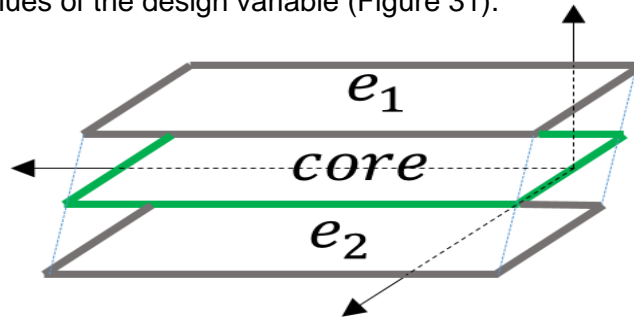


Figure 31 - Composition of the composite based structural components

4.2 Design variables

4.2.1 X position of the spars

Four of the five wing spars, internal reinforcements, change their x position (Figure 32). The distance between the origin of the axis (the leading edge of the UAV wing) and the opposite tip (trailing edge of the UAV wing), is considered as 100%. Within that space, the spars can change their x position, limited by the respectively position of the others. In Figure 33 is possible to see the sequential location of the spars (spar 1, spar 2, spar 3, spar 4 and spar 5).

In the constant section of the wing (Figure 33), the order of the spars in the x axis from 0% to 100% is always: Spar 1, spar 2 and spar 3. By this way, the x position of the spar 1 is limited by the x position of the leading edge and the x position of spar 2. The spar 2 is limited by the x position of spar 3 and that last one is limited by the x position of the trailing edge. In the

narrowing section (Figure 33), there is a fixed spar (spar 5). Its x position in the intrados of the wing is one of the limitations of the x position of the spar 4, being the other one the x position of the leading edge of the wing.

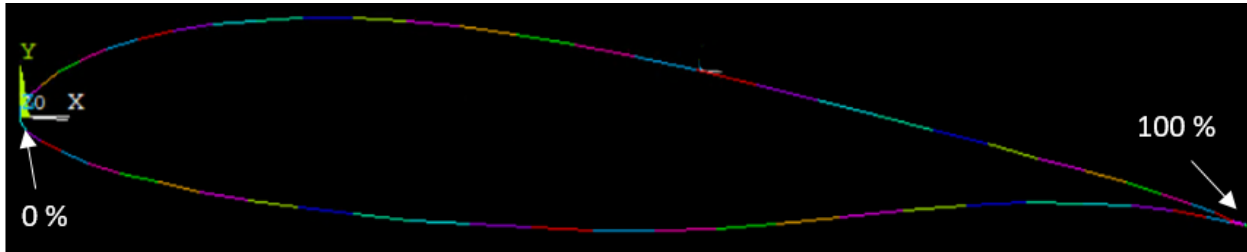


Figure 32 - Wing airfoil (front view) and the coordinated axis (*ANSYS model*)

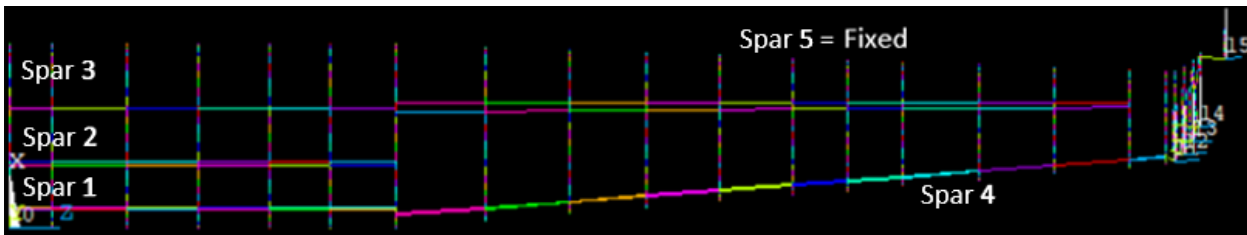


Figure 33 - Spars, ribs and winglet (*ANSYS model*)

By that way, the “ x position %” of the four spars represent four different optimization design variables. Due to manufacture restrictions, considering the wing geometry, it is assumed that the parameters vary between 7 % and 80 %.

The “ x positions %” values was chosen considering the time that each iteration took, the number of different combinations that resulted from those values and the thickness restrictions of the materials. The goal was to have the most possibilities, considering that constraints. The increment step tries to avoid different spars having the same “ x positions %” . When it happens, that solution is not valid once the *ANSYS Mechanical APDL* model was not programmed for that (in the real manufacture process, in “UAVision”, that possibility is not considered with that measurement rigor).

4.2.2 No. Laminas, fibre orientation and material thickness

Several optimization variables were defined due to the material variations in the UAV wing structure. The materials influence directly the maximum deflection and weight values of the wing.

The wing is mostly composed of carbon-epoxy composite and “Airex C70.75”. The “Aluminum 6082 T6” is used in one rib (rib 1), where the fixed end boundary condition is applied.

Associated to the composite material, there are two parameters: The orientation of the fibers ($1 \rightarrow 0^\circ \setminus 90^\circ$ or $2 \rightarrow \pm 45^\circ$) and the number of laminas (0.2 mm of thickness each). Related to the core material foam (“Airex C70.75”), there is only one parameter: Its thickness (mm). In the optimization process was considered its use (thickness $\neq 0 \text{ mm}$) or not (thickness $= 0 \text{ mm}$).

Considering that the external skin is made by carbon-epoxy laminas and each spar (total no. = 5) and rib (total no. = 15) by carbon-epoxy laminas and “Airex C70.75” (as the core material, if its thickness is different from zero), Table 9 resumes the design variables values. Note that of the fifteen ribs only result three parameters, having all the same material characteristics.

Some important notes about Table 9, to clarify any doubts:

- Orientation of the fibers: ($1 \rightarrow 0^\circ \setminus 90^\circ$ or $2 \rightarrow \pm 45^\circ$);
- No. of laminas, e.g. 2, means that there are 2 laminas in each side of the component, so 4 laminas in total ($2 \times 2 \times 0.2 = 0.8 \text{ mm}$). Figure 31;
- Thickness of the core (from 0 mm to 16 mm).

Therefore, there are 24 design variables: 4 (x position of the spars), 2 (material of the exterior skin), 15 (materials of the spars), 3 (materials of the ribs).

4.3 MATLAB and ANSYS Mechanical APDL

4.3.1 MATLAB functions

Table 10 exhibits a scheme of the *MATLAB* functions adapted for this work.

Table 10 - *MATLAB* functions

Function	Description
limpaCACHE.m	It is run before the beginning of a new analysis. Resets all the initial conditions (initial list of points and the nondominated list of points, from the simulation).
Parameters_dms.m	Sets the algorithmic strategies, parameters, constants, and tolerances values to be used by the function “dms.m”, which can be modified by the user.
driver_dms_discreto.m	Applies the DSM algorithm to determine the complete Pareto front for the bound constrained optimization problem. The design variables are defined in this function.
funcFF.m	The objective function values are provided by the <i>ANSYS</i> model (Figure 34).

4.3.2 Functionality

The functionality of the optimization procedure is outlined in Figure 34.

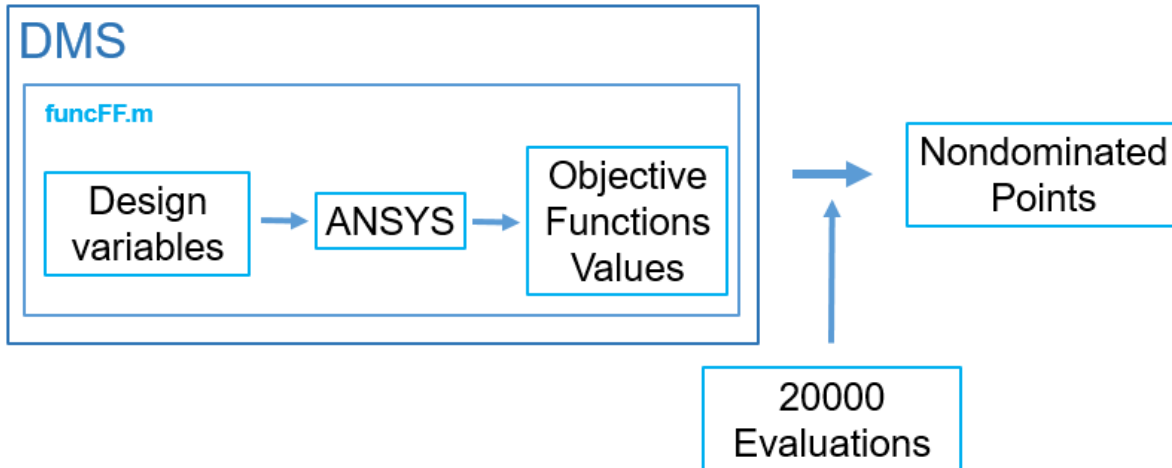


Figure 34 - Functionality of the optimization procedure

The objective functions evaluation is done by the DMS function, “funcFF.m”, where the ANSYS model is used. (Figure 35)

```
Editor - C:\Users\joaferreira\Desktop\Final\funcFF.m
funcFF.m
1 function [F] = funcFF(x)
2
3 delete('saida. ');
4 delete('MASSA_DEFLEXAO.txt');
5 delete('inputvarproj.txt');
6 delete('ansutmp');
7
8 f=fopen('inputvarproj.txt','w');
9 fprintf(f,'%d\r\n%d\r\n%d\r\n%d\r\n%d\r\n%d\r\n%d\r\n%d\r\n%d\r\n%d\r\n%d\r\n%d\r\n%d\r\n%d\r\n%d\r\n%d\r\n%d\r\n',x(1),x(2),x(3),...
10 x(4),x(5),x(6),x(7),x(8),x(9),x(10),x(11),x(12),x(13),x(14),x(15),x(16),x(17),x(18),x(19),x(20),x(24),x(22),x(23),x(24));
11 fclose(f);
12
13 system('SET KMP_STACKSIZE=2048k & "C:\Program Files\ANSYS Inc\v181\ANSYS\bin\winx64\ANSYS181.exe" -b -j saida -dir..._
14 "C:\Users\joaferreira\Desktop\Final" -i "C:\Users\joaferreira\Desktop\Final\PerfilAsa.txt" -o "C:\Users\joaferreira\Desktop\Final\saida.out");
15
16 %criar ficheiro "MASSA_DEFLEXÃO" e escrever "inf", se furox = longx4
17 fid=fopen('MASSA_DEFLEXAO.txt','r');
18 if fid == -1
19     fid=fopen('MASSA_DEFLEXAO.txt','w');
20     A=[inf,inf];
21     fprintf(fid,'%f \n%f',A);
22 end
23 fclose(fid);
24
25 % ler resultados do programa Joao Ferreira 'MASSA_DEFLEXAO.txt'
26 fvalue = fopen('MASSA_DEFLEXAO.txt','r');
27 for i=1 : 2
28     f_num(i) = fscanf(fvalue,'%f',1);
29 end
30 fclose(fvalue);
31 F = [f_num(1) f_num(2)];
32 end
```

Figure 35 – “funcFF.m” function

The input file (that contains the 24 design variables values) is read and interpreted by the ANSYS model (it is “called” and “run” in that function). From that point, the geometry of the wing is generated and the boundary conditions are applied, being the structural simulation of the wing done. The output file is given by the ANSYS model (with the maximum deflection and mass values

of the wing). After 20000 evaluations (the stop criterion), the optimization procedure is finalized. From that procedure are obtained the possible solutions, the nondominated points.

Note: “dms_paretofront.m” is the script that stores the list of nondominated points.

4.3.3 Results from the optimization point of view

The nondominated solutions (points) list obtained from the DMS optimization process was converted into a graph and is showed in Figure 36, where in the x axis are the values of the “min(maximum deflection) [m]” and in the y axis the values of the “min(mass) [kg]”. This is the best approximation achieved, from the optimization point of view, to the Pareto front.

The Pareto front approximation obtained is discontinuous. There are also some regions with a bigger density of points. Some of its sub-regions will be discard based on the needs and goals of the problem in question (as mentioned in “section 2.3.2”).

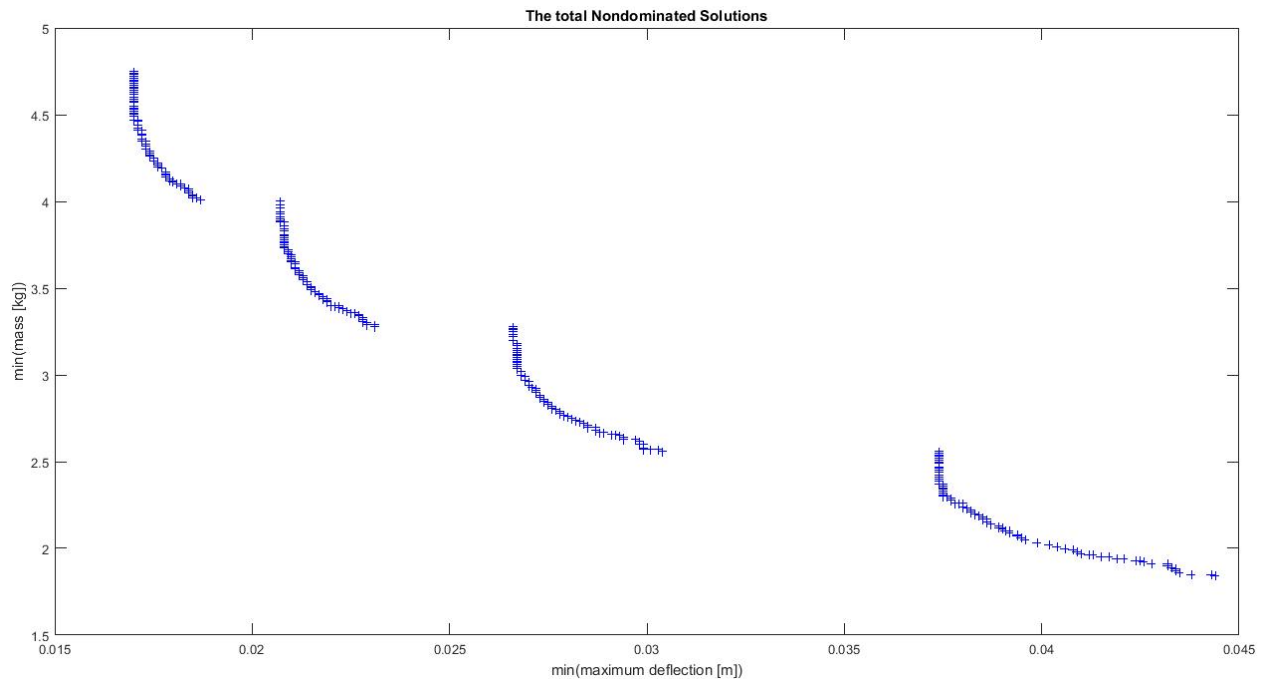


Figure 36 – The total nondominated solutions

Were obtained 358 possible solutions (wing geometries). Since the goal is to minimize both objective functions, the values of the maximum deflection and mass of the wing geometry currently being used will be the limit values. This restriction was not considered during the programming phase because the “UAVision” wanted all the possible solutions, once depending on the mission, are implemented more or less instruments (e.g. cameras) on the wing, being its maximum deflection and mass values variable.

5 Results

5.1 Wing test made in “UAVision”

5.1.1 Characteristics of the wing

Was made in the “UAVision” company a wing test, where were used sandbags (0.5 *kg* each) and a real UAV wing. The purpose of the test was to analyze the behavior of the wing when subject to lifting loads, namely the maximum deflection measured in the winglet tip. The structure of the wing was not the one currently used, having some structural differences. Comparing Figure 37 with Figure 33, is noted that the spars are shorter and differently distributed along the wing.



Figure 37 - Internal structure of the UAV wing tested (courtesy of “UAVision”)

Another important fact is that the current UAV wing is divided in two sections (to facilitate the transportation of the wing), using two carbon-epoxy tubes (fixed end boundary condition) to maintain them together, when assembled. This feature was also not applied in this case. The materials used in the wing are the same as the ones already mentioned in the previous chapters. The finishing manufacturing processes (e.g. painting) were not applied in this wing, too. Also other components like the ailerons, the flaps and the electrical parts where not assembled. Figure 38 shows the exterior aspect of the UAV wing tested.



Figure 38 - Exterior of the UAV wing tested (courtesy of “UAVision”)

5.1.2 Particularities of the test

The components used during the test were (Figure 39):

- UAV wing;
- 0.5 kg sandbags;
- A wing holder;
- Ruler;
- Two people.



Figure 39 - UAV wing test (courtesy of "UAVision")

From the Figure 39, can be seen that the wing was turned upside down and the sandbags placed on it. The distribution of the sandbags simulates the lifting forces distribution that are normally felt (stationary flight conditions), decreasing its intensity from the middle of the wing to the wing tip (Figure 40). The sandbags were placed one by one, following the wing "deflection level". When it reached a critical "level" (measured by a ruler, viewing the wing behaviour), the placement of the sandbags stopped. The wing holder was positioned in the middle part of the UAV wing (place where part of the fuselage is connected).

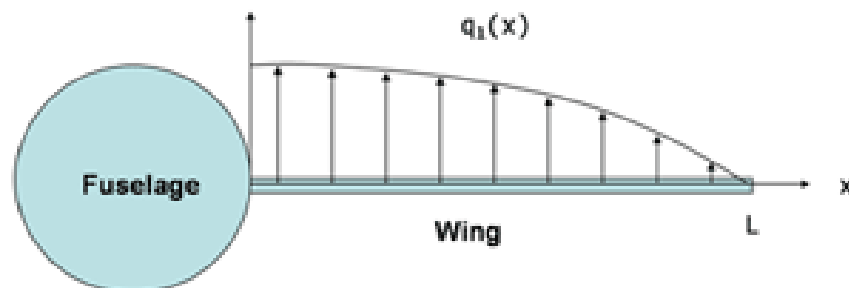


Figure 40 - Lift loads distribution in an aircraft wing [44]

The maximum deflection measured was 200 *mm*. Based on the structural differences, is acceptable that higher value, comparing to the ones from the numerical and optimization results (Figure 37), where the boundary conditions applied and the structure are better approximated to the currently used wing geometry.

5.2 Numerical simulation and optimization results

5.2.1 Characteristics of the wing before the optimization

Half of the current internal UAV wing geometry being used is showed in Figure 41 (the wing is symmetrical). Comparing it with Figure 33, is visible that the internal reinforcement components are similar. A few differences can be noticed in some more complex shapes and in the length and thickness of some of its structural components (was simplified in the *ANSYS* model). In this case, the wing is divided in two (Figure 42, pointed out in red the “division zone”) and the carbon-epoxy tubes are used (fixed end boundary condition), Figure 42.

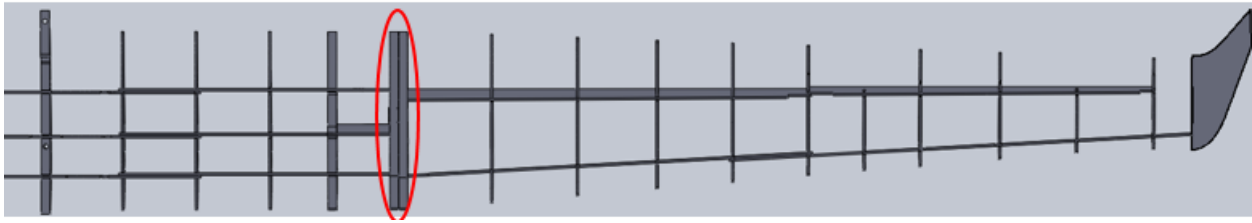


Figure 41 - Current UAV wing geometry *SolidWorks* model (courtesy of “UAVision”)



Figure 42 - Carbon-epoxy tubes (courtesy of “UAVision”)

In Table 11 are some of the optimization design variables values referring to the wing currently used. The (complete) wing is weighing 5 *kg* and the only maximum deflection value measured is the one from the wing test previously mentioned (200 *mm*). That value is not in the order of magnitude expected, due to all the simplifications and missing structural components evidenced before.

Comparing to the wing model from ANSYS, the values of the maximum deflection from the real wing, should be higher. In the numerical model it was modelled a “one-piece wing”, while the real one is divided in two. Related to the weight of the wing, the values obtained from the simulation are expected to be in the same order of magnitude, besides the geometrical approximations and some missing components (like the electrical cables).

Table 11 - Information about the wing geometry currently used (courtesy of “UAVision”)

Detail	Value
Mass	2.5 kg (complete wing: 5 kg)
X position of spar 1	34 %
X position of spar 2	58 %
X position of spar 3	82 %
X position of spar 4	32 %
Carbon fiber Orientation	$\pm 45^\circ$ and $0^\circ/90^\circ$
“Airex C70.75” max thickness	12 mm

Another relevant comparison between the wing currently used and the ANSYS model, is the rib made by aluminum, once it is the densest material in the wing constitution. While in the real wing it has the geometry showed in Figure 43, in the ANSYS model it was approximated to a simpler geometry (Figure 44). At first sight, it is intuitive to think that by this way it will increase considerably the weight results from the optimization process. Whereas, the fact is that the ANSYS model does not consider the weight of the electrical cables and some pieces needed to the ailerons and flaps. As a consequence of that, the weight results from the optimization process are balanced. Note that the rib from the ANSYS model does not have the hole for the carbon-epoxy tube, once it was not considered in the model (the hole is for components like the electrical).



Figure 43 - Aluminum rib in the real wing (courtesy of UAVision)

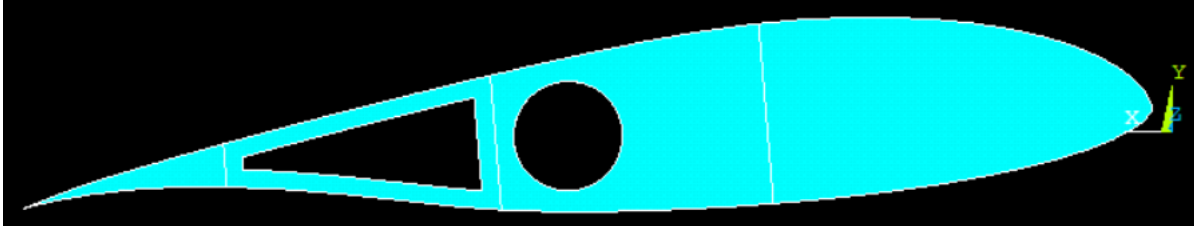


Figure 44 - Aluminum rib in the ANSYS model

Adapting the design variables known from the wing geometry being used (Table 11) to the ANSYS model (half wing), were obtained the following objective functions values (Table 12).

Table 12 - Objective functions values of the current wing geometry (ANSYS simulation)

Objective Function	Value
Maximum deflection	$\approx 0.0375 \text{ m}$
Mass	2.5 kg (complete wing: 5 kg)

From Table 12, can be seen that the mass value is the same as the real wing being used. This simulation confirms the feasibility of the ANSYS model. From now on, the objective functions values obtained (Table 12) from the ANSYS model of the wing geometry currently used are the limit ones (remember that both objective functions should be minimized).

5.2.2 Interpretation of the results

The results from the optimization process already showed in Figure 36, must be analyzed and verified. Is important to remind that the goal of using the DMS solver is to minimize the wing maximum deflection value and its mass (priority), both at the same time. Two criterions were used to delimitate and verify the region of possible solution points acceptable:

- Values of maximum deflection and mass from the current wing used;
- The ultimate tensile stress value of the carbon – epoxy composite materials, considering the tensile tests and the literature ([8]).

Knowing that the “complete” wing currently used weights 5 kg (Table 12) and that the results from the optimization process refer to half of the wing, the maximum value of weight acceptable from the optimization results must be under 2.5 kg (red line in Figure 45). Due to that fact, three of the four regions of nondominated points have to be discarded, the ones above the red line in Figure 45 (see “section 4.3.3”). At this point, considering just the mass limitation, there

are no constraints in terms of the maximum deflection value, since it was proved that an incomplete structure withstands considerably larger deflection values than the ones obtained from the optimization process (see “section 5.1.2”). Because of that, is possible to limit the range of possible values acceptable for this problem based on the points affected by the weight constraint. It is represented with two green lines in Figure 45 (from $\approx 0.0374\text{ m}$ to $\approx 0.0444\text{ m}$). Note that the precision of the values is ensured by the “dms_paretofront.m”.

From the 358 possible solutions there are now 81 solutions acceptable for the problem, delimited by the red and green lines in Figure 45.

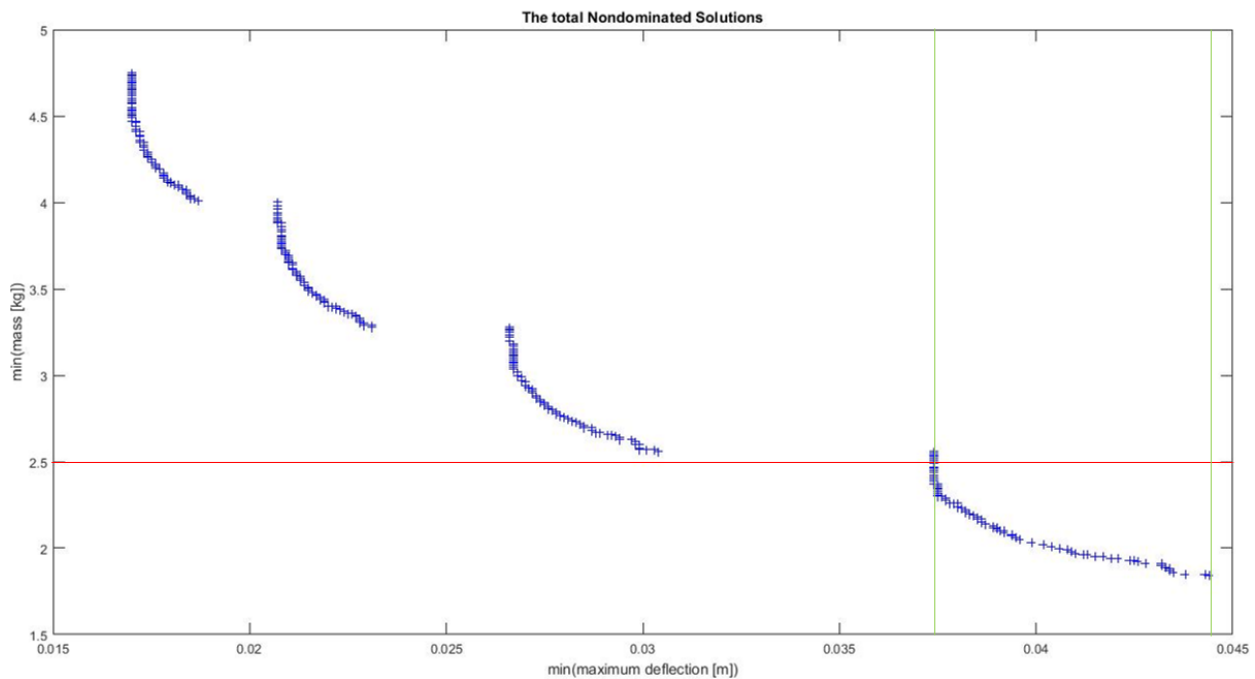


Figure 45 - All the possible solutions

Considering now the simulation results of the maximum deflection from the Table 12, of the 81 possible solutions are considered 17 as acceptable (Figure 46). In Figure 46 are marked (red and blue lines) the current wing geometry objective function values (from the *ANSYS* simulation (Table 12)), delimiting those 17 acceptable solutions (point A to point C). This decrease on the number of solutions happens once is expected to minimize both objective functions, with greater importance to the wing mass.

Of those 17 acceptable solutions, were chosen 3 to be analysed: Point A, point B and point C. Point A and point B once they are the two “end points” of the 17 acceptable solutions,

i.e., point A has the highest minimized maximum deflection value ($\approx 0.0375 \text{ m}$) and the lowest minimized mass value (2.3 kg), while the point C has the opposite, minimized maximum deflection value of $\approx 0.0374 \text{ m}$ and minimized mass value of 2.49 kg . The point B is the one with its objective functions values (min(mass): 2.37 kg ; min(maximum deflection): $\approx 0.0374 \text{ m}$) between the other two (with both objective functions values lower than the current wing objective functions values). The wing geometry characteristics correspondently to those points are evidenced in Table 13.

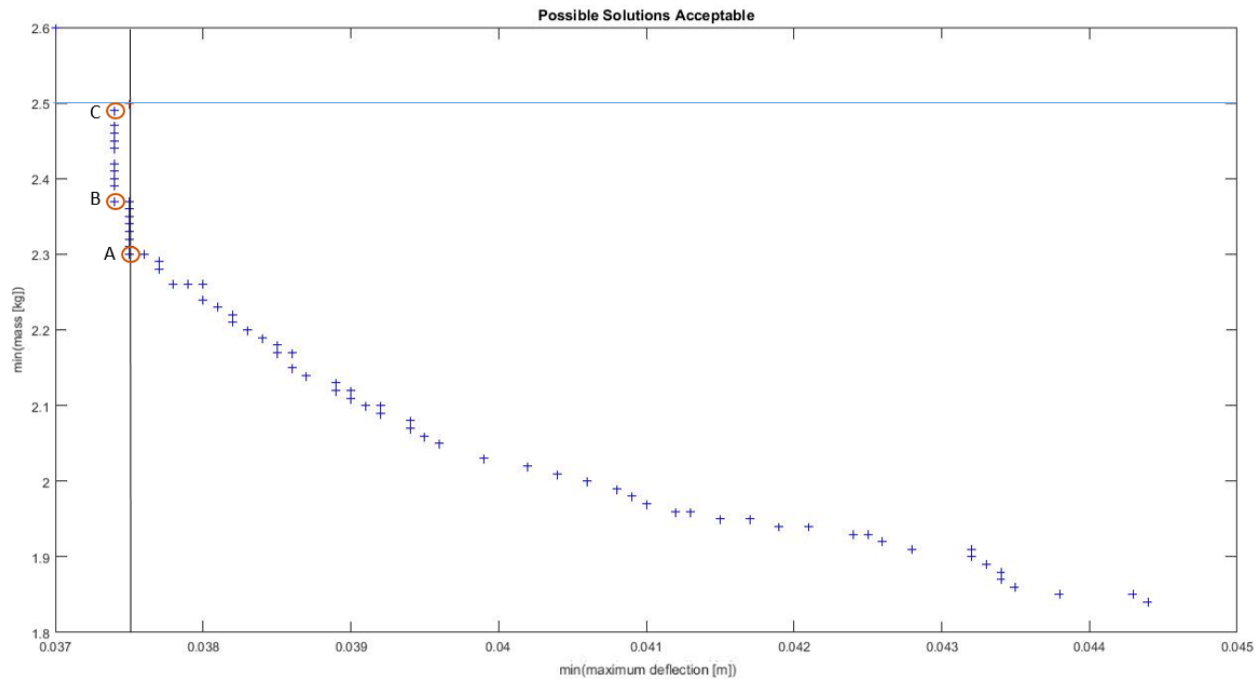


Figure 46 - Possible solutions acceptable

Looking to Table 13, in terms of the design variables values, all the three wing geometries chose (point A, B and C) are considerably similar. Related to the minimized mass values (half wing), point A has the minimum value, while the point C has the maximum (difference of 0.19 kg between those two acceptable solutions). Their minimized maximum deflection values are similar. The x position of the spars is the same for those three geometries. Comparing it to the ones from the current wing being used (Table 11), is noticed that the x position values of the spars 2 and 3 are the ones with a bigger difference. While in the current wing geometry the spars are more distributed and close to the trailing edge of the UAV wing ($32 \% \text{ to } 80 \%$), in the optimized ones they are located more in the center region of the wing ($30\% \text{ to } 65\%$) (Figure 47). By this way the spars are higher (higher inertial \Rightarrow lower stress), reducing the number of laminas used (\Rightarrow lower mass value). Comparing the number of carbon-epoxy laminas and the orientation of the carbon fibres in the structural components (Table 13), there are no considerable differences.

Table 13 – Wing geometry characteristics of point A, B and C.

Description	Point A	Point B	Point C
Mass ($\frac{1}{2}$ wing):	2.3 kg	2.37 kg	2.49 kg
Max deflection:	≈ 0.0375 m	≈ 0.0374 m	≈ 0.0374 m
Spar 1:	30 %	30 %	30 %
Spar 2:	40 %	40 %	40 %
Spar 3:	65 %	65 %	65 %
Spar 4:	35 %	35 %	35 %
No. Laminas ext. skin:	2 each side (total: 4)	2 each side (total: 4)	2 each side (total: 4)
Orientation fibres skin:	0°/90°	0°/90°	0°/90°
No. Laminas spar 1:	5 each side (total: 10)	5 each side (total: 10)	5 each side (total: 10)
Thickness core spar 1:	0 mm	12 mm	12 mm
Orientation fibres spar 1:	0°/90°	0°/90°	0°/90°
No. Laminas spar 2:	5 each side (total: 10)	5 each side (total: 10)	5 each side (total: 10)
Thickness core spar 2:	4 mm	16 mm	16 mm
Orientation fibres spar 2:	0°/90°	0°/90°	0°/90°
No. Laminas spar 3:	5 each side (total: 10)	5 each side (total: 10)	5 each side (total: 10)
Thickness core spar 3:	0 mm	4 mm	4 mm
Orientation fibres spar 3:	0°/90°	0°/90°	0°/90°
No. Laminas spar 4:	5 each side (total: 10)	5 each side (total: 10)	5 each side (total: 10)
Thickness core spar 4:	0 mm	0 mm	4 mm
Orientation fibres spar 4:	0°/90°	0°/90°	0°/90°
No. Laminas spar 5:	4 each side (total: 8)	5 each side (total: 10)	2 each side (total: 4)
Thickness core spar 5:	0 mm	16 mm	0 mm
Orientation fibres spar 5:	$\pm 45^\circ$	$\pm 45^\circ$	0°/90°
No. Laminas ribs:	3 each side (total: 6)	2 each side (total: 4)	2 each side (total: 4)
Thickness core ribs:	0 mm	0 mm	0 mm
Orientation fibres ribs:	0°/90°	0°/90°	0°/90°

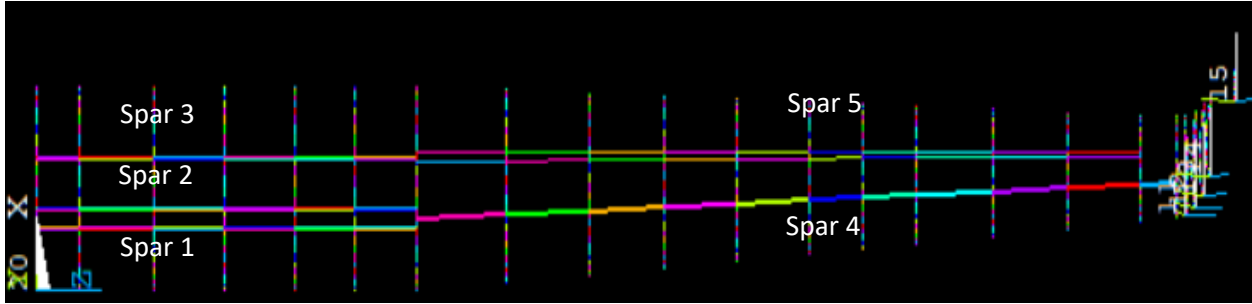


Figure 47 - Position of the spars, point A, B, C (ANSYS model)

It is prioritized the minimization of the mass. Of the 17 acceptable solutions, the point A corresponds to the optimal wing geometry from the optimization process. Besides having an approximated maximum deflection value ($\approx 0.0375\text{ m}$) to the one from the current wing geometry, its mass minimization corresponds to a decrease of 8%. Based on that, is expected to have a “complete” wing weighting 4.6 kg , instead of the prior 5 kg . Related to the minimization of the maximum deflection wing value, the maximum decrease achieved is with the point C ($\approx 0.0374\text{ m} \rightarrow 0.3\% \text{ decrease}$). Those remarks are summarized in Table 14.

Table 14 - Results remarks

Objective Function	Description (complete wing)
min(maximum deflection)	max decrease of 0.3 %
min(mass)	max decrease of 0.4 kg (8%)

To validate those three solutions (Point A, B and C), generalizing its analysis results to the other 14 acceptable solutions, was done a structural analysis using the ANSYS model. Knowing from the tensile tests done (“section 3.1.4”) that the ultimate tensile stress value of the “epoxy + bi carbon fiber $+45^\circ/-45^\circ$ ” is 100 MPa and considering that the “epoxy + bi carbon fiber $0^\circ/90^\circ$ ” showed a better mechanical behavior, that value was considered as the critical one. As it is showed in Table 13, the only wing component with the “epoxy + bi carbon fiber $+45^\circ/-45^\circ$ ” is the spar 5, in the point A and B (wing geometry solutions). By this way, was verified the tensile stresses there.

In Figure 48 is exhibited the tensile stress values (green) in the spar 5 of the (wing geometry) point A. As can be seen, the maximum value of tensile stress is 5.46 MPa ($< 100\text{ MPa}$). From the Figure 49 can be seen the tensile stress values (green) for the point B (wing

geometry). The maximum tensile stress value is 5.21 MPa ($< 100 \text{ MPa}$). By this way, is verified the structural behavior of the “epoxy + bi carbon fiber $+45^\circ/-45^\circ$ ” based wing components.

The maximum tensile stress values, considering the entire wing, are showed in Figure 50, Figure 51 and Figure 52 (point A, point B and point C respectively). All these three geometries show their maximum tensile stress values in the skin (“epoxy + bi carbon fiber $0^\circ/90^\circ$ ”) of the wing, in the fixed end zone. This result was expected and the tensile values (A – 86.9 MPa ; B – 86.2 MPa ; C – 86.5 MPa) are still lower than 100 MPa . Since from the tensile tests made there are no information for the ultimate tensile stress for the “epoxy + bi carbon fiber $0^\circ/90^\circ$ ”, but was verified that it bore higher loads, can be extrapolate the viability of the structure by this way.

The results obtained with the point A, point B and point C were generalized for the other 14 acceptable solutions. Between the 17 acceptable solutions, the design variables values don't have a considerable variation, being reasonable this approach.

From now on, is expected the manufacture and test of the point A (the optimal wing geometry obtained), in order to validate it experimentally (it was not possible to be done during this work, due to the unavailability of “UAVision”).

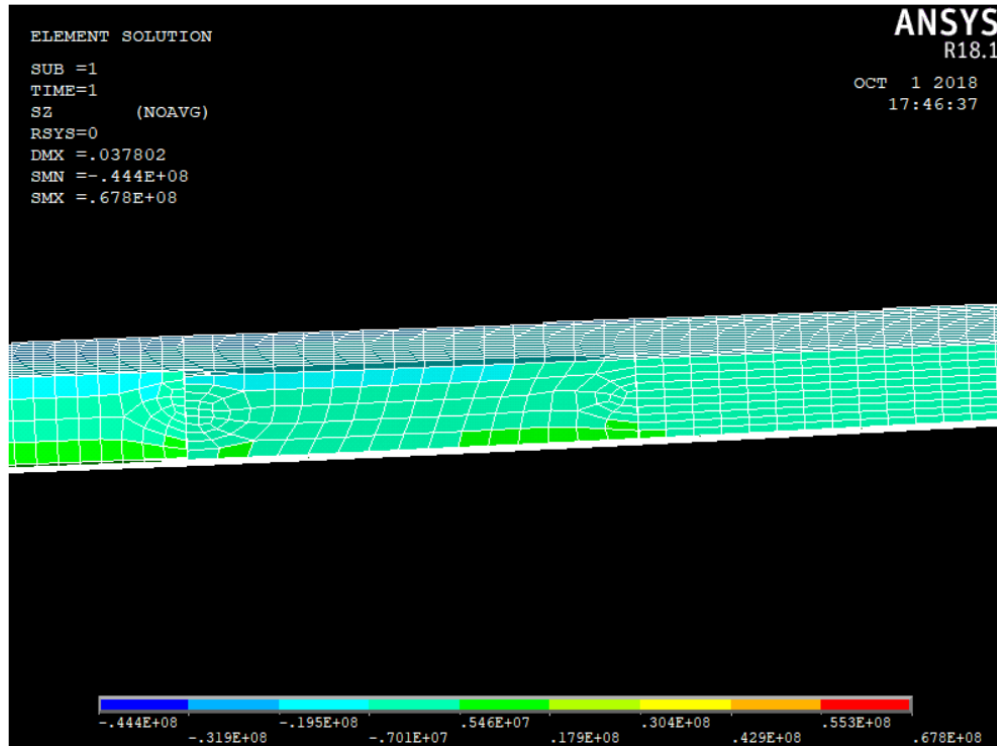


Figure 48 - Tensile stress values of spar 5, point A (ANSYS model)

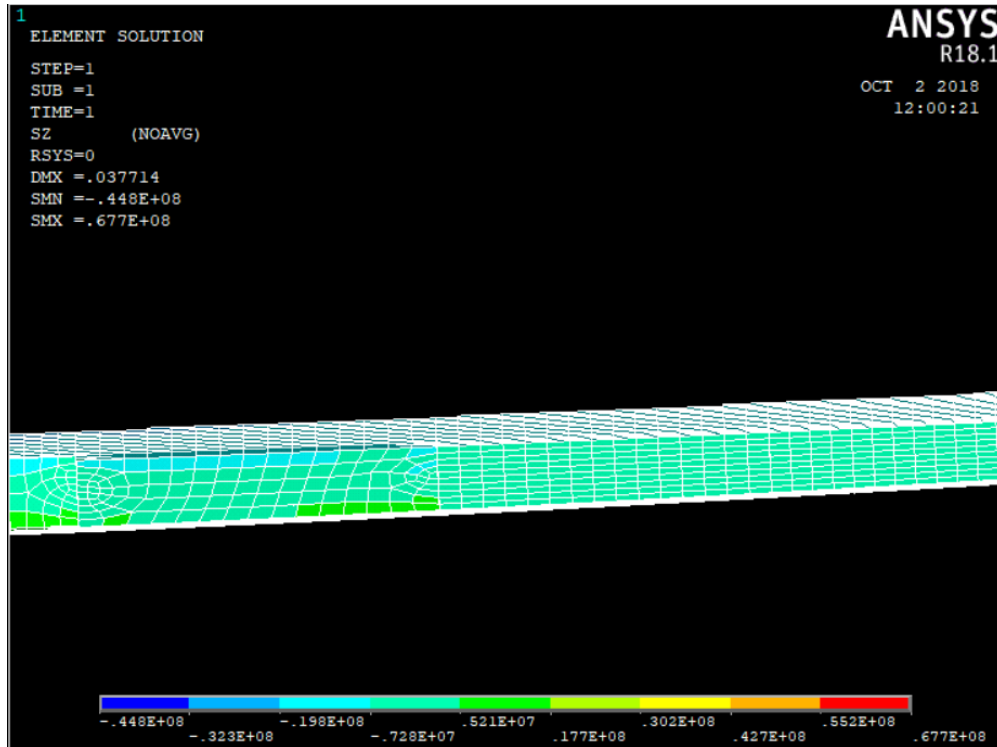


Figure 49 - Tensile stress values of spar 5, point B (ANSYS model)

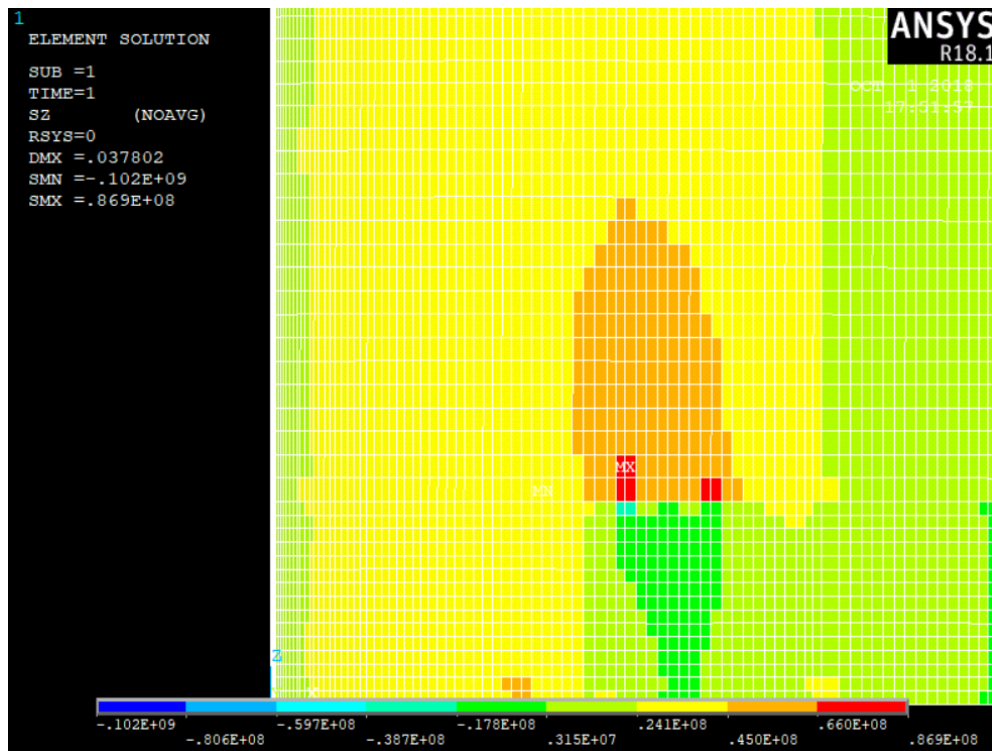


Figure 50 - Maximum tensile stress value, point A (ANSYS model)

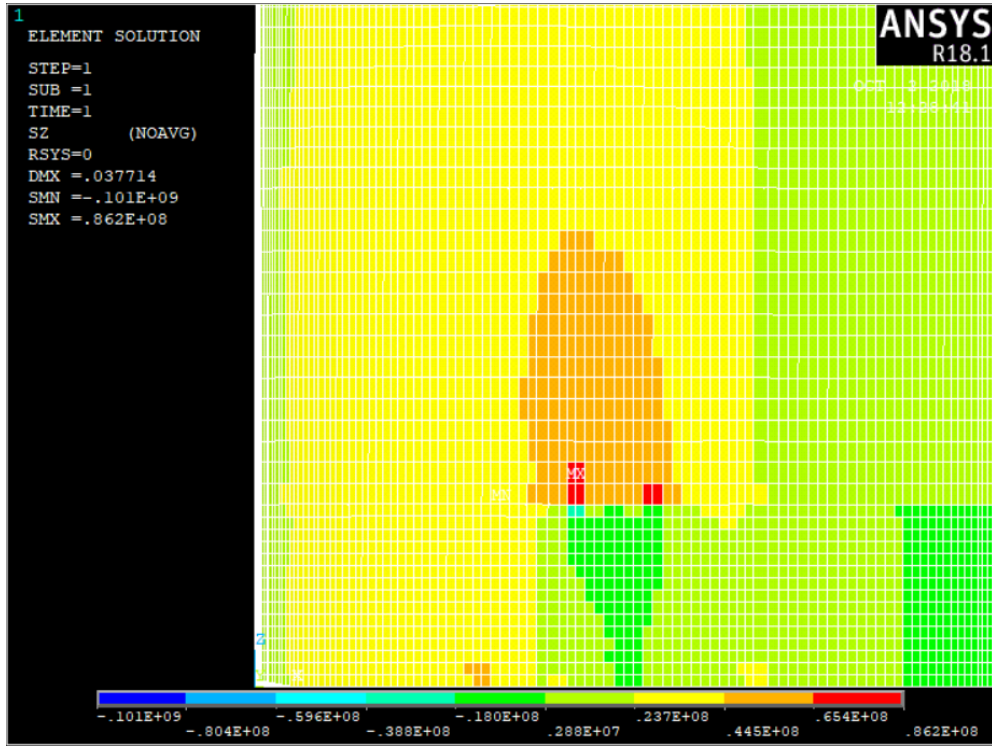


Figure 51 - Maximum tensile stress value, point B (ANSYS model)

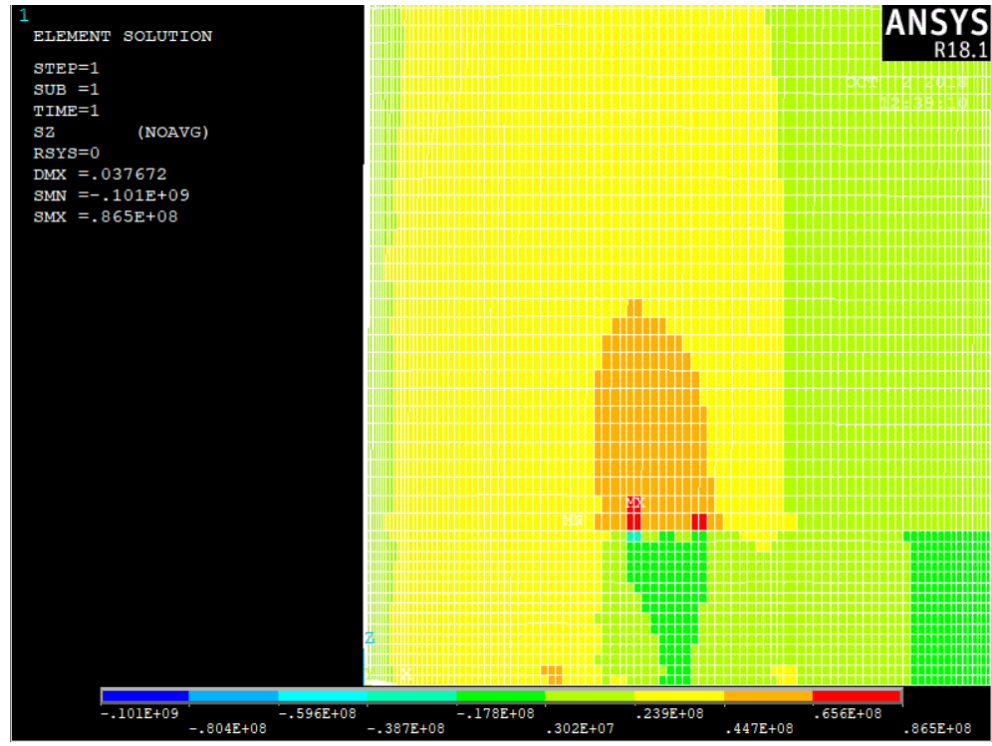


Figure 52 - Maximum tensile stress value, point C (ANSYS model)

6 Production of the Wing

All the process from the design to the assemble of the UAV components (like the wing) is made by "UAVision". To manufacture and assemble one single UAV wing, as the one in study, are needed three weeks.

6.1 Wing components

In this section is described in a summarized way the production of the main structural components of the wing, evidencing the manufacture process, the tools and some surface finishes applied. To be more understandable, the information will be exhibit in topics (illustrated by some figures).

- 1) The exterior skin of the wing is divided in two, the top part and the bottom part. To made them, the first thing produced are the molds (Figure 53). It is used a rigid foam and a robot (Figure 54) to shape the exterior wing skin parts on it. Having the molds, the carbon-epoxy exterior wing skin is laminated (hand lay-up and vacuum cure). At the same time, in a separate section, the "carbon-epoxy + Airex C70.75" ribs and spars (in the case of having the core materials) are made (hand lay-up and vacuum cure);

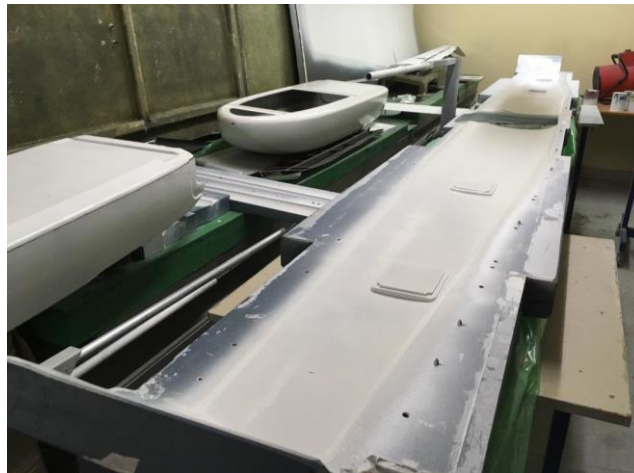


Figure 53 – Wing molds (courtesy of "UAVision")

- 2) The interface between the fuselage and the wings is manufactured. The ribs and the spars are cut, using a CNC machine like the "Hass VF-4SS" (Figure 24);
- 3) At this point, some finishing details start to be applied. The exterior wing skin parts are trimmed (handmade procedure). Using a mechanical lathe (Figure 55), the interface region between the wing and the tail boom is made.



Figure 54 – Robot (courtesy of “UAVision”)



Figure 55 - Mechanical lathe (courtesy of “UAVision”)

- 4) The bottom part of the exterior wing skin is glued (structural “MI-05” glue) with the fuselage, ensuring the connection between these two UAV parts.

6.2 Assembly

In this section are mentioned the main assembly steps of the UAV wing in study. The room where the carbon-epoxy components are prepared (Figure 56) and the painting room (Figure 57) are showed.

- 1) The bottom part of the exterior skin is placed on a bench. The ribs and the spars are placed on the skin, being posteriorly glued together with the structural “M1-05” glue;
- 2) The ribs and the spars are glued to the bottom part of the skin (“M1-05” glue);

- 3) The carbon-epoxy tubes that connect the wing to the tail boom are placed and aligned;
- 4) The carbon-epoxy tubes, fixed end boundary condition, are installed (Figure 42);
- 5) Some cuts are made in the zone of the flaps and of the ailerons (trailing edge of the wing).
The structural components of that two parts are installed;
- 6) All the electronic cables are installed and connected to the respective parts;
- 7) The top part of the wing is placed and glued with the bottom parts ("M1-05" glue);
- 8) The wing is painted;
- 9) All the tops needed (e.g. the tops of the servos) are installed on the wing;
- 10) The exterior wing skin is cut in two (in the region already mentioned in "section 5.2.1"),
in order to facilitate its transportation.



Figure 56 - Carbon-epoxy room (courtesy of "UAVision")



Figure 57 - Painting room (courtesy of "UAVision")

7 Conclusions and Future Works

Conclusions

The present work was an opportunity to work directly with a company, the “UAVision”. By this way was possible to deal with a real need of the company, working in an engineering environment, namely in a place where the design and the manufacture of their products is done. The fact of being with the engineers and the workers in the production area, make possible to understand and experience the routines and dynamics of the company.

This work was presented by me in the "6th International Conference on Engineering Optimization", that took place in “Técnico Lisboa”, between the 17th and 19th of September of 2018 (Figure 58, Annexes).

Related to the 3D modelling phase, using the *ANSYS* software (*Mechanical APDL* interface), several geometrical approximations were done, in order to simplify the problem due to restrictions of time. Those simplifications affected the maximum deflection values (model: “one-piece wing”; real wing: divided in two). Besides that, the values obtained from the optimization process were acceptable. Not having a previous test made with the current wing geometry (in the structural point of view), resulted in a lack of information for comparison with the values from the model. Related to the mass values obtained, and comparing it with the ones known from the real wing, they were in the same scale of values. Based on the similarities with the real wing, in terms of the materials used and the structural components of the wing, the mass results were expected to be quite satisfactory. Note that were considered stationary flight conditions for the distributed forces applied on the wing.

In the optimization process was used the DMS solver. Were considered 24 design variables taking into account the materials of the structural components and the x position of the spars. The discrete values were chosen considering the thickness of the wing components and the wing geometry possibilities. For this stage was used the *MATLAB* software (inside the DMS solver, the *ANSYS* model was executed). Were obtained several wing geometries, with different values of maximum deflection and mass. The results proved once again that this solver can be used in practical examples and that it is functional. Were considered as acceptable solutions 17 wing geometries (from the initial 358), from which the optimal one corresponds to a reduction of 0.4 kg of mass (complete wing), while the maximum deflection value maintained approximately the same as the one from the current wing geometry (from the *ANSYS* model result ($\approx 0.0375 m$)). In this type of structures, maintaining the structural components and the materials,

this reduction of weight is considerable and improves the performance of the vehicle. In terms of the maximum deflection value, there was no big reduction (0.3%). However, since there was not enough information (maximum deflection) about the current wing geometry, there are no further conclusions besides the ones already mentioned.

Related to the carbon fiber orientation, the “epoxy + bi carbon fiber 0°/90°” was the preferred. Based on its higher young’s modulus and its mechanical behavior (better than the “epoxy + bi carbon fiber +45°/-45°”), this result was expected.

Based on the optimized wing geometries analyzed (point A, B, C) was verified that the spars were tendentiously located more to the center of the wing (x position), when compared to the geometry currently used. In fact, that location make them (the spars) higher, increasing their inertia momentum and as a consequence decreasing the stresses. By this way is possible to reduce the number of carbo-epoxy laminas in their constitution and as a consequence cause a decrease in the weight of the wing. Note that the spars are subjected mainly to bending. These solutions were verified based on the tensile stress analysis, using the *ANSYS* model. That verification was generalized for the other 14 acceptable solutions, since there were not verified considerable differences between those wing geometries.

Based on the work done and the results obtained, the objectives were accomplished, namely in terms of the mass reduction. The DMS solver was applied correctly and the 3D wing model (*ANSYS*) programmed corresponds to a viable wing approximation.

Future works

In order to validate the optimized solutions obtained from the simulation process is expected to manufacture the optimal wing geometry (point A) and test it, never discarding the other 16 acceptable solutions.

To improve the simulation results, the 3D model can be improved. All the geometrical approximations should be taken into account, namely divide the wing in two (affect mainly the maximum deflection values) and implement the carbo-epoxy tubes (fixed end boundary condition).

From the optimization point of view, the number of the discrete design variable values can be increased (decreasing the increment step, considering the materials thickness restrictions). By that way the number of possible solutions expected should be higher than the one obtained.

Related to the carbon fiber orientation, should be tested the use of unidirectional fibers.

References

- [1] Bone, E., Bolkcom, C. (2003). Unmanned Aerial Vehicles: Background and Issues for Congress Current. Report for congress, Congressional Research Service. The Library of Congress
- [2] Sullivan, J. M. (2006). Evolution or revolution? The rise of UAVs. IEEE Technol. Soc. Mag, vol. 25, pp. 43 - 49
- [3] Pereira, E., Bencatel, R., Correia, J., Félix, L., Gonçalves, G., Morgado, J., Sousa, J. (2009). Unmanned Air Vehicles for Coastal and Environmental Research. Journal of Coastal Research. Proceedings of the 10th International Coastal Symposium ICS 2009, vol. 2, pp. 1557-1661
- [4] Nomani, K. (2007). Prospect and Recent Research & Development for Civil Use Autonomous Unmanned Aircraft as UAV and MAV. Journal of System Design and Dynamics, vol. 1, pp.120-128
- [5] UAVision. (2018). Website of UAVision Company, <https://www.uavision.com/>, accessed at the 6th of July.
- [6] Niu, M. C. (2000). Airframe structural design: practical design information and data on aircraft structures. ISBN 962-7128-04-x
- [7] Custódio, A. L., Madeira, J. F. A., Vaz, A. I., F., Vicente, L. N. (2011). Direct Multisearch for Multiobjective Optimization. SIAM J.Optim., vol. 21, pp. 1109-1140
- [8] Performance composites. (2018). Website of Performance Composites Ltd., http://www.performance-composites.com/carbonfibre/mechanicalproperties_2., accessed at the 12th of March.
- [9] Core Materials. (2018). Website of Airex AG., <http://www.airexag.ch/de/startseite.html.>, accessed at the 12th of March.
- [10] Aluminium Alloy. (2018). Website of Aalco Metals Ltd., http://www.aalco.co.uk/datasheets/Aluminium-Alloy_6082-T6~T651_148.ashx., accessed at 12th of March.
- [11] Jones, R. M., Bert, C. W. (1999). Mechanics of Composite Materials (2nd ed.). Taylor and Francis. ISBN:1-56032-712-X
- [12] Chawla, K. K. (2012). Composite Materials Science and Engineering (3rd ed.). Springer. ISBN 978-0-387-74364-6
- [13] Reddy, J. N. (2004). Mechanics of Laminated Composite Plates and Shells – Theory and Analysis (2nd ed.). Boca Raton: CRC PRESS. ISBN 0-8493-1592-1.
- [14] Campbell, F. C. (2010). Structural Composite Materials. ASM International. ISBN 978-1-

61503-037-9

- [15] Islam, M., Mahdi, T. H., Hosur, M. V., Jeelani, S. (2015). Characterization of carbon fiber reinforced epoxy composites modified with nanoclay and carbon nanotubes. *Procedia Engineering*. Elsevier. ScienceDirect, vol. 105, pp. 821 - 828
- [16] VASILIEV, V. V., MOROZOV, E. V. (2001). *Mechanics and Analysis of Composite Materials*. (1st ed.). Oxford: Elsevier Science Ltd. ISBN 0-08-042702-2.
- [17] Craver, C. D., Carraher, C. E. (2000). *Applied Polymer Science 21st Century*. (1st ed.). Elsevier Science Ltd. ISBN 0 08 04341177
- [18] Mouritz, A. P. (2012). *Introduction to aerospace materials*. (1st ed.). Woodhead Publishing Ltd. ISBN 978-0-85709-515-2
- [19] Quilter, A. (2004). *Composites in Aerospace Applications*. IHS ESDU.
- [20] Rezende, M., Botelho, E. (2000). O uso de compósitos estruturais na indústria aeroespacial. *Polímeros: Ciência e Tecnologia*, vol 10, nº 2, pp. e4 - e10. ISBN 0104-1428
- [21] Chung, D. D. L. (2010). *Composite Materials Science and Applications* (2nd ed.). Springer. ISBN 978-1-84882-830-8
- [22] Dooly, G., Omerdic, E., Coleman, J., Miller, L., Kaknjo, A., Hayes, J., Braga, J., Ferreira, F., Conlon, H., Barry, H., Marcos-Olaya, J., Tuohy, T., Sousa, J., Toal, D. (2016). Unmanned vehicles for Maritime spill response case study: Exercise Cathach. *Elsevier Ltd. Marine Pollution Bulletin*, vol. 110, pp. 528-538.
- [23] Karma, S., Zorba, E., Pallis, G. C., Statheropoulos, G., Balta, I., Mikedi, K., Vamvakari, J., Pappa, A., Chalaris, M., Xanthopoulos, G., Statheropoulos, M. (2015). Use of unmanned vehicles in search and rescue operations in forest fires: Advantages and limitations observed in a field trial. Elsevier Ltd. *International Journal of Disaster Risk Reduction*, vol. 1, pp. 307-312
- [24] Samad, T., Bay, J. S., Godbole, D. (2007). Network-centric systems for military operations in urban terrain: The role of UAVs. *Proceedings of the IEEE*. ISBN 0018-9219
- [25] Mohammed, F., Idries, A., Mohamed, N., Al-Jaroodi, J., Jawhar, I. (2014). UAVs for Smart Cities: Opportunities and Challenges. *International Conference on Unmanned Aircraft Systems (ICUAS)*. Conference Proceedings, pp. 267 - 273. ISBN 9781479923765
- [26] Bendsøe, M. P., Sigmund, O. (2003). *Topology optimization: Theory, methods and applications* (2nd ed.). Springer. ISBN 3-540-42992-1
- [27] Xu, Y., Zhu, J., Wu, Z., Cao, Y., Zhao, Y., Zhang, W. (2018). A review on the design of laminated composite structures: constant and variable stiffness design and topology optimization. Springer International Publishing AG

- [28] Arora, J. (2011). Introduction to Optimum Design (3rd ed.). Academic Press. Chapter 17. ISBN 9780123813763
- [29] Handl, J., Kell, D. B., Knowles, J. (2007). Multiobjective optimization in Bioinformatics and Computational Biology. IEEE/ACM Transactions on Computational Biology and Bioinformatics, vol. 4, pp. 279 - 292
- [30] Deb, K. (2001). Multi-objective Optimization Using Evolutionary Algorithms (1st ed.). John Wiley & Sons, LTD. ISBN 0-471-87339-X
- [31] Ribeiro, V. H. A., Reynoso-Meza, G., Coelho, L. S. (2017). Multi-objective Model Selection for Unmanned Aerial Vehicles Automatic Target Recognition Systems. Elsevier Ltd. IFAC-PapersOnLine, vol. 50, pp. 11607 - 11612
- [32] Deb, K. (1999). Multi-objective Genetic Algorithms: Problem Difficulties and Construction of Test Problems. International Journal of Conflict Management. MIT. Evolutionary Computation, vol. 7, pp. 205 - 230
- [33] Custódio, A. L., Emmerich, M., Madeira, J. F. A. (2012). Recent Developments in Derivative-free Multiobjective Optimization. Computational Technology Reviews, vol. 5, pp. 1-30
- [34] Madeira, J. F. A., Araújo, A. L., Mota Soares, C. M., Mota Soares, C. A. (2014). Multiobjective optimization of viscoelastic laminated sandwich structures using the Direct Multisearch method. Elsevier Ltd. Computer and Structures, vol. 147, pp. 229-235
- [35] Monte, S. M. C. (2015). Previsão do Comportamento e Otimização de um Componente Estrutural de Aeronaves em Material Compósito. Dissertação de Mestrado em Aeronáutica Militar na Especialidade de Engenharia Aeronáutica, Técnico Lisboa, Universidade de Lisboa
- [36] Silva, J. J. M. (2017). Design and Optimization of a Wing Structure for a UAS Class I 145 kg. Master Thesis in Military Science Aeronautical Engineering, Técnico Lisboa, Universidade de Lisboa
- [37] Correia, V. M. F., Madeira, J. F. A., Araújo, A. L., Soares, C. M. M. (2016). Multiobjective design optimization of laminated composite plates with piezoelectric layers. Composite Structures, vol. 169, pp.10-20
- [38] Santos, A. M. A. (2017). Dynamic analysis and design of impact attenuator structures for a Formula Student prototype. Master thesis in Mechanical Engineering, Técnico Lisboa, Universidade de Lisboa
- [39] Figueiredo, I. M. P. (2016). Previsão do Comportamento Mecânico e Otimização de Placas

- em Material Compósito Híbrido. Dissertação de Mestrado em Engenharia Aeroespacial, Técnico Lisboa, Universidade de Lisboa
- [40] Ramos, M. H. S. (2015). Construction and Analysis of a Lightweight UAV Wing Prototype. Master thesis in Aerospace Engineering, Técnico Lisboa, Universidade de Lisboa
- [41] Dlugosz, A., Kilmek, W. (2018). The Optimal Design of UAV Wing Structure. AIP Conference Proceedings, vol. 1922, pp. 120009-1 - 120009-8
- [42] INSTRON. (2018). Website of Illinois Tool Works Inc., <http://www.instron.us/en-us>, accessed at the 23rd of August.
- [43] Faria, L., Sousa, L. (2015). Mecânica dos Sólidos Notas das aulas e problemas. Departamento de Engenharia Mecânica. Técnico Lisboa
- [44] Technical Articles and Newsletters. (2018). Website of The Mathworks Inc., <https://www.mathworks.com/company/newsletters/articles/analytical-modeling-of-aircraft-wing-loads-using-matlab-and-symbolic-math-toolbox.html>., accessed at 28th of August.

Annexes



Figure 58 - Certification of attendance at EngOpt2018